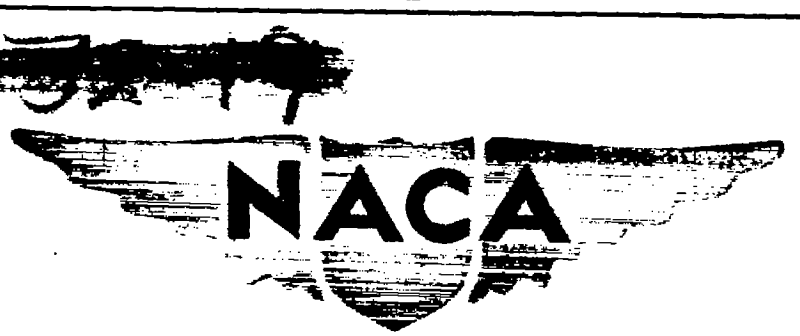

RESEARCH MEMORANDUM

FLIGHT-TEST EVALUATION OF THE LONGITUDINAL STABILITY AND CONTROL CHARACTERISTICS OF 0.5-SCALE MODELS OF THE LARK PILOTLESS-AIRCRAFT CONFIGURATION

By

David G. Stone

Langley Memorial Aeronautical Laboratory
Langley Field, Va.

NATIONAL ADVISORY COMMITTEE FOR AERONAUTICS

WASHINGTON
February 6, 1948

Classification cancelled (or changed to Unclassified)

By Authority of Navy Tech Pub Announcement #109
(REF TO AUTHORIZED TO CHANGE)

By 29 NOV. 56

NK
(GRADE OF OFFICER MAKING CHANGE)

4 Apr 61
DATE

NATIONAL ADVISORY COMMITTEE FOR AERONAUTICS

RESEARCH MEMORANDUM

FLIGHT-TEST EVALUATION OF THE LONGITUDINAL STABILITY AND CONTROL CHARACTERISTICS OF 0.5-SCALE MODELS OF THE LARK PILOTLESS-AIRCRAFT CONFIGURATION

By David G. Stone

SUMMARY

Flight tests were conducted at the Flight Test Station of the Pilotless Aircraft Research Division at Wallops Island, Va., to determine the longitudinal stability and control characteristics of 0.5-scale models of the Lark pilotless aircraft. The investigation included tests of the standard configuration (tail surfaces interdigitated with respect to the wings) having the horizontal wing flaps deflected 0°, 15°, and 60° and a test with the tail surfaces in line with the wings with wing flaps not deflected. The data were obtained by the use of radio telemeters and by radar tracking.

All the configurations tested possess static longitudinal stability. The stability decreases slightly up to approximately the critical Mach number, but with further increase in Mach number the stability increases severely. All the configurations tested exhibited dynamic longitudinal stability with the exception of some dynamic instability indicated for the standard configuration, flaps deflected 60°, and for the tail in line with the wings configuration.

Aerodynamic reversal of the longitudinal trimming control occurs for the standard configuration with flaps not deflected and with a flap deflection of 15°. For the 0° flap deflection, the reversal occurs suddenly at a Mach number of 0.93 and continues to the maximum speed obtained of 0.98. For the 15° flap deflection a reduction in control effectiveness begins at a Mach number of 0.75 and gradually decreases, becoming negative at a Mach number of 0.89.

Placing the tail in line with the wings results in a considerable reduction in the trimming-control effectiveness.

The aerodynamic lag of the trimming control encountered in the tail-in-line configuration and the standard configuration with 60° flap deflection would make angle-of-attack stabilization extremely difficult.

The abrupt changes in the longitudinal acceleration indicate large drag increases at critical Mach numbers of 0.80 for 0° flap deflection and 0.75 for the 15° flap deflection (standard configurations).

INTRODUCTION

The NACA conducted flight tests of the Lark pilotless-aircraft configuration to evaluate the longitudinal stability and control characteristi at high subsonic speeds. To obtain this information, 0.5-scale models, externally geometrically similar to the Lark missiles, were constructed at NACA and flown at the Flight Test Station of the Pilotless Aircraft Research Division at Wallops Island, Va. This paper covers the results of all the flight tests. The results reported herein pertain to the longitudinal characteristics of the standard Lark configuration having the wing flaps deflected 0°, 15°, and 60° and of a configuration with the tail surfaces in the same plane with respect to the wings having the wing flaps not deflected.

The full-scale Lark missile is designed to be flown at zero angle of attack and sideslip for the seeker reference; the lift and side-force increments for maneuvering are to be gained by deflection of the horizontal and vertical wing flaps; and the rudder-elevator control surfaces are to be used as trimmers only. In these model tests the control surfaces produced angle of attack, but tests with various wing-flap deflections provided data for an evaluation of the effectiveness of the trimming-control function. The models were flown with a programmed flicker-type deflection of the longitudinal trimming-control surfaces.

SYMBOLS

t	time from launching, seconds
M	free-stream Mach number
p	free-stream static pressure, pounds per square foot
q	free-stream dynamic pressure, pounds per square foot $\left(\frac{\gamma}{2}pM^2\right)$
H	free-stream total pressure, pounds per square foot
C_N	normal-force coefficient $\left(\frac{a_n}{g}\frac{W}{S}\frac{1}{q}\right)$
C_C	chord-force coefficient $\left(\frac{a_l}{g}\frac{W}{S}\frac{1}{q}\right)$

$\frac{dM}{d\alpha}$	rate of change of pitching moment with angle of attack, foot-pounds per radian
$\frac{dC_m}{d\alpha}$	rate of change of pitching-moment coefficient with angle of attack, per degree
$\frac{dC_L}{d\alpha}$	rate of change of lift coefficient with angle of attack, per degree
$\frac{\Delta\left(\frac{a_n}{g}\right)}{\Delta\delta_e}$	change of normal acceleration with elevator deflection, per degree
$\frac{dC_m}{d\delta_e}$	rate of change of pitching-moment coefficient with elevator deflection, per degree
$\frac{dC_L}{d\delta_e}$	rate of change of lift coefficient with elevator deflection, per degree
$\frac{dC_N}{d\delta_e}$	rate of change of normal-force coefficient with elevator deflection, per degree
$\left(\frac{d\delta_e}{d\delta_f}\right)_{C_L=k}$	rate of change of elevator deflection required for trim with flap deflection at constant lift coefficient
$\left(\frac{dC_m}{d\delta_f}\right)_{C_L=k}$	rate of change of pitching-moment coefficient with flap deflection at constant lift coefficient, per degree
P	period of oscillation, seconds
I_y	moment of inertia about Y-axis, slug-feet^2
W	weight of model, pounds
S	horizontal wing area, 2.725 square feet
c	wing chord, 0.883 foot
a_l	longitudinal acceleration, feet per second per second
a_n	normal acceleration, feet per second per second

g	acceleration of gravity, 32.2 feet per second per second
δ_f	deflection of horizontal wing flaps, degrees
δ_e	deflection of rudder-elevators or elevators, degrees (trailing edge down is positive)
γ	specific heat ratio; value taken, 1.4

MODELS AND APPARATUS

Models

The 0.5-scale models used for this investigation were externally geometrically similar to the full-scale Lark pilotless-aircraft configuration. The models were simplified over the full-scale version in that they did not have automatic pilots, seekers, ailerons, or remote-control systems. The model fuselages and components were constructed of duralumin, aluminum castings, and magnesium skin. The fuselage construction was of the monocoque type separable into three sections. The three sections are: the nose section which holds the telemeter and batteries; the center section which holds the rocket motor, wings, and compressed-air supply; and the tail section which holds the control system, tails, and blast tube. The model horizontal wings were made of laminated micarta and the vertical wings were made of laminated beech. The tails were made of laminated micarta, and all the control surfaces were of solid magnesium.

The models were propelled by a dry-fuel, Cordite, 5-inch-diameter rocket motor which is capable of producing thrust varying from 1000 pounds to 1400 pounds depending upon the ambient temperature and the manufacturing qualities. The use of a blast tube was necessary to locate the rocket-motor center of gravity on approximately the desired model center-of-gravity position. From tests made on a static thrust stand, the blast tube had little effect on the thrust characteristics (unpublished data).

Figure 1 presents the general arrangement of the model representing the standard configuration, tail interdigitated with respect to the wings. Photographs of this model and rocket motor with blast tube are shown in figure 2. Figure 3 presents the general arrangement of the model having the tail surfaces in the same plane as the wings. A photograph of this model with rocket motor and blast tube is shown in figure 4.

The programmed movement of the rudder-elevators was accomplished by a compressed-air system with a flicker-type operation. The control surfaces moved together between stops in a square wave motion at frequencies of approximately one-half or three-fourths of a cycle per second. This

control motion was in operation before the models left the launcher and all during the flight. Figure 5, a tail-view photograph of the model, shows the deflected control surfaces and the end of the blast tube. The tail-in-line tests were accomplished by rotating the tail section, fastening the vertical control surfaces at 0° deflection, and connecting the servosystem to the horizontal control surfaces which were then elevators.

Tests were made with the horizontal wing flaps deflected 0°, 15°, and 60°. Details of the 0.20-chord plain-type flap deflected 60° are shown in figure 6. The moment of inertia about the Y-axis was found by swinging the models by the tail as shown in figure 7.

All the models were ground-launched without a booster on a zero-length launcher set at angles of either 30° or 45° from level. Photographs of the models on the launcher are presented in figure 8. Photographs of the launching of the standard configuration model are shown in figure 9, and figure 10 presents the launching of the tail-in-line model.

The general specifications and weight and balance of all the models as compared to the full-scale aircraft are presented in table I and in table II. The test conditions at the times of the launching of the models were as follows:

Configuration	Sea-level pressure (lb/sq ft)	Speed of sound (ft/sec)	Approximate crosswind velocity (ft/sec)	Approximate launching angle (deg)
$\delta_f = 0°$	2144	1124	0	30
$\delta_f = 15°$	2131	1142	6	45
$\delta_f = 60°$	2122	1142	9	30
$\delta_f = 0°$; tail in line	2141	1136	16	45

Apparatus

The data from the flights were obtained by the use of telemeters, CW Doppler radar and photography. The four-channel radio telemeter gave continuous signals of the longitudinal acceleration, normal acceleration, impact pressure, and the control-surface position. A photograph of the radio-transmitter part of the telemeter system is shown in figure 11.

Two independent telemeter receiving stations recorded the radio-transmitted data. The telemeter records were converted to the accelerations and control positions directly by use of preflight calibration results. The impact pressure records from the telemeters were reduced to Mach number by the following equation:

$$M^2 = \frac{2}{\gamma - 1}\left[\left(1 - \frac{H - p}{H}\right)^{-\frac{\gamma-1}{\gamma}} - 1\right] \qquad (1)$$

where p was taken as the pressure at sea level at the time of the test. Since the models reached an altitude of only about 500 feet, no large errors in M are introduced by taking p constant.

The CW Doppler radar served as a check on the velocity obtained from the telemeter records. Photography served as an observation for any structural failure or any flight peculiarities.

TECHNIQUE

The technique of introducing a disturbance about the Y-axis of a body in free flight and analyzing the resultant forces and accelerations was used for the investigation of the longitudinal stability characteristics. The disturbance in this case was the continuous operation of the longitudinal control surfaces in a square-wave flicker-type operation. The models did not contain any automatic stabilization systems. Rolling of the model does not affect the validity of the normal accelerometer reading in that it always reads the actual load normal to the plane of the wings regardless of roll attitude.

METHODS OF ANALYSIS

The telemeter and radar records were reduced to time-history records of the flight as plots of Mach number, control position, and normal and longitudinal accelerations versus time from launching. The normal acceleration and longitudinal acceleration were reduced to normal-force coefficient and chord-force coefficient, respectively. From plots of a_n/g against M an indication of the effectiveness of the control surfaces was gained by determining the change in a_n/g for the change in δ_e or $\frac{\Delta\left(\frac{a_n}{g}\right)}{\Delta\delta_e}$ and comparing these values as the static stability changed with Mach number and configuration. An indication of the control effectiveness of the full-scale Lark is gained by the term normal-acceleration factor, $\frac{\Delta\left(\frac{a_n}{g}\right)}{\Delta\delta_e}\left(\frac{W}{S}\right)$. In order to obtain the normal

acceleration produced per degree of elevator control deflection for any desired wing loading, divide the normal-acceleration factor by the desired wing loading. The normal-acceleration factor and the normal-force coefficient were based on a linear variation with time of the wing loading from the take-off condition to the burnout condition.

Evaluations of the static longitudinal stability were obtained by analysis of the short-period oscillations induced by the abrupt movement of the elevator control. These short-period oscillations appeared in the normal-acceleration curve in the time-history records. The period of the motion for small amplitudes may be expressed as a function of the moment of inertia and the restoring moment per radian movement with respect to the relative wind as follows:

$$P = 2\pi\sqrt{\frac{I_y}{dM/d\alpha}} \tag{2}$$

or

$$\frac{dC_m}{d\alpha} = -\frac{4\pi^2 I_y}{57.3\ P^2 qSc} \tag{3}$$

The second-order effects, such as the amplitude of the oscillation, were found to have no appreciable effect on the value of the period. However, the effect of damping due to pitching velocity is not included, and, if the damping factor is large, some error may be expected. This method of analysis of the short-period oscillations for the determination of static stability is similar to that reported in reference 1 for determining the directional stability from flight records. The values of $dC_m/d\alpha$ obtained are for model-flight center-of-gravity locations which varied approximately 2 percent chord between models and approximately 1 percent chord for each model. A similar variation of the moment of inertia was included in the computation of $dC_m/d\alpha$ for each case.

Approximations of the effectiveness of the trimming control may be gained by evaluating the rate of change of pitching moment with control deflections as follows:

$$\frac{dC_m}{d\delta_e} = -\frac{\Delta\left(\frac{a_n}{g}\right)}{\Delta\delta_e}\,\frac{W}{qS}\,\frac{\frac{dC_m}{d\alpha}}{\frac{dC_L}{d\alpha}} \tag{4}$$

Evaluations by equation (4) assume an average value of $dC_L/d\alpha$ and that the normal-force coefficient is equivalent to the lift coefficient.

RESULTS AND DISCUSSION

Time-History Records

Standard configuration; $\delta_f = 0^\circ$.- A time history of the flight of a 0.5-scale model Lark with the tail interdigitated with respect to the wings and wing flaps not deflected is presented in figure 12. The total elapsed flight time was 5.64 seconds with approximately $2\frac{1}{2}$ oscillations of the rudder elevators. The maximum speed obtained corresponded to a Mach number of 0.98 (rocket burnout) at a time of 4.03 seconds after launching. The dashed portion of the longitudinal-acceleration curve was obtained by differentiation of the velocity curve. This was done because of failure of the telemeter receiver to record properly this channel until a time of 3.4 seconds was reached.

Figure 13 presents the variation of normal-force coefficient with Mach number for the power-on flight period. Figure 14 presents curves of chord-force coefficient and normal-force coefficient against Mach number for the power-off decelerating portion of the flight.

Standard configuration; $\delta_f = 15^\circ$.- A time history of the flight of a model with the horizontal wing flaps deflected 15° is presented in figure 15. The total elapsed flight time was 9.60 seconds. The maximum speed corresponded to a Mach number of 0.92 (rocket burnout) at a time of 3.7 seconds after launching. The dashed part of the Mach number curve was obtained by integration of the longitudinal-acceleration curve.

Figure 16 presents the variation of normal-force coefficient with Mach number for the power-on part of the flight. The maximum value of C_N obtained is near the stalled region for the Lark configuration. Figure 17 presents curves of chord-force and normal-force coefficients for the power-off decelerating part of the flight.

Standard configuration; $\delta_f = 60^\circ$.- A time history of the flight of a model with the horizontal wing flaps deflected 60° is presented in figure 18. The total elapsed flight time was 17.9 seconds. As determined from visual and photographic observation, the model began a slow roll near $t = 1.8$ indicating that the right wing flap loosened resulting in unknown deflections, and near $t = 7.0$ the right wing flap broke off causing a severe roll. Further record conversion beyond the time the flap broke off was considered unnecessary. The maximum speed obtained

corresponded to a Mach number of 0.91 (rocket burnout) at a time of 3.78 seconds after launching. The dashed Mach number curve was obtained by integration of the longitudinal acceleration. For this flight the total head channel and the Doppler radar failed to record properly.

Figure 19 presents the variation of normal-force coefficient with Mach number for the power-on flight period. Figure 20 presents curves of chord-force and normal-force coefficients for the power-off decelerating part of the flight.

Tail-in-line configuration; $\delta_f = 0^\circ$.- A time history of the flight of a 0.5-scale model Lark with the tail in line with the wings and $\delta_f = 0^\circ$ is presented in figure 21. The total elapsed flight time was 40.8 seconds. Only the first 8 seconds of the flight were presented since after this time no change in the recorded characteristics was noted until the compressed air for the servosystem was expended a few seconds later. The maximum speed obtained corresponded to a Mach number of 0.87 (rocket burnout) at $t = 3.86$. The dashed Mach number curve was obtained by integration of the longitudinal acceleration with the initial point at $t = 2.4$ where the data from the total head channel and the radar check exactly. The low maximum velocity as compared with that shown for the standard configuration can be attributed to poor rocket thrust as indicated by $a_l \approx 7g$ as compared with $a_l \approx 9g$ in previous tests. After $t = 3.8$ the total head channel failed to record properly, and the recording time of the radar was expended at $t = 3.6$.

Figure 22 presents the variation of normal-force coefficient with Mach number for the power-on flight period. Figure 23 presents curves of chord-force and normal-force coefficients for the power-off decelerating part of the flight.

Drag

Referring to figure 12, record of the model with wing flaps not deflected, the large decrease in longitudinal acceleration during powered flight which occurs at $M = 0.8$ $(t = 2.9)$ indicates a large increase in the drag. Also, the drag remained high, as indicated by the immediate deceleration during the power-off flight. Unpublished high-speed wind-tunnel data from tests of this configuration show a large drag increase near $M = 0.8$, the critical Mach number.

Again a large increase in the drag is indicated for the $\delta_f = 15^\circ$ configuration (refer to fig. 15) by the decrease in the longitudinal acceleration at high normal accelerations near $M = 0.75$. Also, the higher value of C_C above $M = 0.75$ as compared to those at lower values of M indicates the drag increase.

An indication of the drag rise with Mach number for the tail-in-line configuration may be shown by considering that where $C_N = 0$ the C_C is equivalent to the drag coefficient. As shown in figure 23, at $M = 0.81$ ($t = 4.79$) the drag coefficient is 0.069 decreasing to 0.033 at $M = 0.73$ ($t = 7.56$).

Longitudinal Stability

Static stability.- The values of the period of the short-period oscillation induced by the sudden control movement determined from the time-history records are presented in figure 24 to show the variation of the period with Mach number. The scatter of the test points on figure 24 indicates the amount of error in determining P. The considerable scatter for the $\delta_f \approx 60^\circ$ configuration may be due to loosening of the flap.

Figure 25 presents the static longitudinal stability, as computed using equation (3), as a function of Mach number. For the standard configuration, as M increases, the stability decreases slightly; then as M increases further, the stability increases severely, especially after the critical Mach number. For the tail-in-line configuration the static stability is less at low Mach numbers but increases faster and is greater as M increases, as compared with the tail interdigitated with the wings. These data indicate that the static longitudinal stability changes rapidly with lift coefficient and Mach number. In general, deflecting the flaps reduces the static stability at low Mach numbers, but the large increases in the stability near the critical speed occur at lower Mach numbers than without deflection of the flaps.

By taking the value of the slope of the lift curve $dC_L/d\alpha$ to be 0.08 (unpublished wind-tunnel data), and including the variation of center of gravity, the neutral points were computed for these conditions. These neutral points, of course, do not include the probable changes in $dC_L/d\alpha$ beyond the critical Mach number. The variation of the neutral points with M for all the configurations tested is given in figure 26. Again the increase in stability is indicated by the large rearward movement of the neutral point as M increases above 0.70.

Dynamic stability.- A qualitative evaluation of the dynamic stability may be determined by inspection of the damping of the short-period oscillation induced by the abrupt control movement. Referring to the time-history records, figures 12, 15, 18, and 21, the following comparison may be made of the average time for complete damping of the oscillation:

Configuration	Control dwell time (sec)	Average time for complete damping (sec)	
		Positive g	Negative g
$\delta_f = 0^\circ$	1.1	0.8	0.5 to 0.7
$\delta_f = 15^\circ$	1.8	0.8	0.8
$\delta_f \approx 60^\circ$	0.6	Not damped in dwell time	Undamped oscillation during dwell time
$\delta_f = 0^\circ$; tail in line	0.6	0.4 to not damped in dwell time	0.3

The tendency for the dynamic instability for the $\delta_f \approx 60^\circ$ configuration may be caused by the slippage of the wing flap.

Control Effectiveness

Control reversal.- Referring to figure 12, time-history record of standard configuration $\delta_f = 0^\circ$, it may be seen that the normal acceleration, with the usual short-period oscillation, followed the deflection of the rudder-elevators until a Mach number of 0.93 was reached. At $M = 0.93$, with 6.5° up-elevator, the normal acceleration suddenly changed from a positive value of $4\frac{1}{2}g$ to a negative value of $4g$. This reversal of longitudinal control continued as the speed increased to $M = 0.98$. Control was fully reestablished when the speed decreased to $M = 0.92$. The cause of this control reversal may be attributed to any combination of the following high-speed effects: (1) shift of the angle of zero lift of the cambered horizontal wing, (2) loss of rudder-elevator effectiveness, (3) reversal of tail effectiveness at small rudder-elevator deflections because of a shift of the angle of zero lift of the effectively cambered tail, and (4) wing-wake effects. Tests by RM-5 rocket-propelled models of 0.2-chord, plain ailerons on a straight wing, 9 percent thick (reference 2), indicate a similar phenomenon by showing an abrupt reduction in rolling control effectiveness at the same speeds.

Again for the flight of the standard configuration $\delta_f = 15^\circ$ a reversal of the longitudinal control was encountered. Referring to figure 15, it may be seen that the normal acceleration, with the usual short-period oscillations, followed the deflection of the rudder-elevators until a Mach number of 0.75 was reached ($t \approx 2.6$). With approximately 8.5° up-elevator, the normal acceleration changed from a positive value of about 20g at $M = 0.75$ to a negative value of 5g at $M = 0.92$. As the speed decreased from $M = 0.92$ ($t \approx 4.2$), the longitudinal control was gradually reestablished. Control was fully restored when the speed decreased to $M = 0.75$ ($t \approx 5.3$). The results show an increase of effectiveness of the longitudinal

control in producing normal accelerations up to $M = 0.75$ where this effectiveness gradually decreased, becoming negative at $M = 0.89$.

The effects of this aerodynamic control reversal on the stability of an autopilot system would be such as to cause the missile to diverge from a stabilized flight path. The reduction in control effectiveness preceding the reversal would further complicate the automatic stability problem.

For the standard configuration $\delta_f \approx 60^\circ$ and the tail-in-line configuration $\delta_f = 0^\circ$ no reversal of the longitudinal control was encountered.

Ability of control to produce normal acceleration.- The ability of the longitudinal control surfaces to produce normal acceleration is shown in figure 27 as plots of a_n/g against M. The dashed lines are the interpolation of the data between regions of the same control deflection. The differences between curves of power-on and power-off flight were probably caused by thrust misalinement with the center of gravity. The normal-acceleration-producing ability, or change in a_n/g for the change in δ_e, $\frac{\Delta\left(\frac{a_n}{g}\right)}{\Delta\delta_e}$, as determined from figure 27 is given in figure 28.

The normal acceleration producing capabilities of the control surfaces of the Lark missile configuration for any wing loading are presented in figure 29 as a plot of normal-acceleration factor $\frac{\Delta\left(\frac{a_n}{g}\right)}{\Delta\delta_e}\left(\frac{W}{S}\right)$ against Mach number. For example, at $M = 0.75$ the following comparisons of the normal accelerations produced per degree of elevator deflection may be made:

δ_f	0.5-scale model			Full-scale aircraft		
	W/S (lb/sq ft)	Center of gravity (percent chord)	a_n/g per δ_e	W/S (lb/sq ft)	Center of gravity (percent chord)	a_n/g per δ_e
0°	38.9	16.64	-0.86	110	16.64	-0.30
15°	36.6	19.81	-1.95	110	19.81	-.65
60°	39.2	18.60	-1.20	110	18.60	-.43
0°; tail in line	38.4	18.60	-.26	110	18.60	-.09

It is evident that placing the tail in line with the wings results in an appreciable reduction in the normal acceleration producing capabilities. The changes in control effectiveness for the tail-in-line configuration and the $\delta_f \approx 60^\circ$ configuration may be attributed to wake effects from the wing affecting the tail surfaces.

An estimation of the control effectiveness in terms of $dC_m/d\delta_e$ may be gained by the use of equation (4) assuming the value of the slope of the lift curve. For example, at $M = 0.75$, assuming $\frac{dC_L}{d\alpha} = 0.08$, the following values of $dC_m/d\delta_e$ may be obtained:

δ_f	$dC_m/d\delta_e$
0°	-0.016
15°	-0.022 (high C_N)
60°	-0.017 (high C_N)
0°; tail in line	-0.004

Aerodynamic lag.- Also shown in the time-history records (figs. 12, 15, 18, and 21), the production of normal acceleration lags the application of control deflection. For the standard configuration $\delta_f = 0^\circ$ and $\delta_f = 15^\circ$, the lag in produced normal acceleration is approximately 0.05 second. Placing the tail in line with the wings increased the lag time to 0.10 and to 0.15 second. Similarly, deflecting the wing flap 60° increased the lag time to over 0.10 second. This aerodynamic lag in the effectiveness of the controls may be due to wake interference from the wing. The aerodynamic lag of the trimming control encountered in the tail-in-line configuration and the standard configuration flaps deflected 60° is such as to make angle-of-attack stabilization on the full-scale missile very difficult.

Wing flap effect on trim.- An estimation of the effect of wing flap deflection on the pitching-moment coefficient at constant lift at a given Mach number may be gained by considering the following:

$$\left(\frac{dC_m}{d\delta_f}\right)_{C_L=k} = \frac{dC_m/d\alpha}{dC_L/d\alpha}\frac{dC_L}{d\delta_e}\left(\frac{d\delta_e}{d\delta_f}\right)_{C_L=k} \tag{5}$$

where

$$\frac{dC_L}{d\delta_e} = \frac{dC_N}{d\delta_e} = \frac{\Delta\left(\frac{a_n}{g}\right)}{\Delta\delta_e}\frac{W}{qS} \tag{6}$$

The term $\left(\frac{d\delta_e}{d\delta_f}\right)_{C_L=k}$ may be determined from figure 27 by evaluating the δ_e required for $\frac{a_n}{g} = k$ at a given Mach number using the $\delta_f = 0^\circ$ configuration for the reference. Therefore the rate of change of pitching-moment coefficient with flap deflection at constant lift is

$$\left(\frac{dC_m}{d\delta_f}\right)_{C_L=k} = \frac{\frac{dC_m}{d\alpha}}{\frac{dC_L}{d\alpha}}\left[\frac{\Delta\left(\frac{a_n}{g}\right)}{\Delta\delta_e}\frac{W}{S}\right]\frac{1}{\frac{\gamma}{2}pM^2}\left(\frac{d\delta_e}{d\delta_f}\right)_{C_L=k} \tag{7}$$

For example, using equation (7), computing at $M = 0.75$ for $\frac{a_n}{g} = 0$ and assuming $\frac{dC_L}{d\alpha} = 0.08$, $\left(\frac{dC_m}{d\delta_f}\right)_{C_L=0} = -0.00004$ for $\delta_f = 15^\circ$ and 0.00006 for $\delta_f \approx 60^\circ$. The positive sign for the $\delta_f \approx 60^\circ$ configuration indicates the large increase in wake effects upon the tail accompanying the large flap deflection. The magnitudes of the values show that wing flap deflection causes no large changes in trim near zero lift.

RECOMMENDATION

Angle of attack.- It is recommended that all models to be used for the study of longitudinal stability and control be equipped with angle-of-attack instrumentation. The addition of an angle-of-attack indicator on models tested in free flight would remove most of the assumptions and errors in the quantitative calculations of the stability and control effectiveness.

CONCLUSIONS

From the results of flight tests of 0.5-scale models to evaluate the longitudinal stability and control characteristics of the Lark pilotless-aircraft configuration, the following general conclusions are indicated:

1. All the configurations tested possess static longitudinal stability. The stability decreased slightly up to approximately the critical Mach number, but with further increase in Mach number the stability increased severely. Also the data indicate that with wing flaps deflected the stability changes with increasing lift coefficient as well as with Mach number.

2. All the configurations tested exhibited dynamic longitudinal stability with the exception of some dynamic instability indicated for the standard configuration (tail interdigitated) $\delta_f \approx 60^\circ$ and for the tail in line with the wings configuration.

3. Reversal of the longitudinal trimming control occurs for the standard configuration with $\delta_f = 0^\circ$ and $\delta_f = 15^\circ$. For the $\delta_f = 0^\circ$ case, the reversal occurs suddenly at $M = 0.93$ and continues to the maximum speed obtained of $M = 0.98$. For the $\delta_f = 15^\circ$ case, a reduction in control effectiveness begins at $M = 0.75$ and gradually decreases becoming negative at $M = 0.89$.

4. Placing the tail in line with the wings results in a considerable reduction in the trimming control effectiveness.

5. The aerodynamic lag of the trimming control encountered in the tail-in-line configuration and the standard configuration, $\delta_f \approx 60^\circ$ would make angle-of-attack stabilization extremely difficult.

6. The abrupt changes in the longitudinal acceleration indicate large drag increases at critical Mach numbers of 0.8 for $\delta_f = 0^\circ$ and 0.75 for $\delta_f = 15^\circ$ (standard configurations).

Langley Memorial Aeronautical Laboratory
National Advisory Committee for Aeronautics
Langley Field, Va.

REFERENCES

1. Bishop, Robert C., and Lomax, Harvard: A Simplified Method for Determining from Flight Data the Rate of Change of Yawing-Moment Coefficient with Sideslip. NACA TN No. 1076, 1946.

2. Sandahl, Carl A., and Marino, Alfred A.: Free-Flight Investigation of Control Effectiveness of Full-Span 0.2-Chord Plain Ailerons at High Subsonic, Transonic, and Supersonic Speeds to Determine Some Effects of Section Thickness and Wing Sweepback. NACA RM No. L7D02, 1947.

TABLE I.- GENERAL SPECIFICATIONS

Item	Full-scale aircraft	0.5-scale models	
		Standard configuration	Tail-in-line configuration
Fuselage:			
Over-all length, in.	164	82	82
Maximum diameter, in.	17	8.5	8.5
Wings:			
Aspect ratio	3.49	3.49	3.49
Total span, in.	74	37	37
Chord (constant), in.	21.2	10.6	10.6
Angle of incidence, deg	0	0	0
Dihedral, deg	0	0	0
Sweep, deg	0	0	0
Airfoil section:			
Horizontal wing	NACA 16-209	NACA 16-209	NACA 16-209
Vertical wing	NACA 16-009	NACA 16-009	NACA 16-009
Wing area (per pair including fuselage), sq ft	10.9	2.725	2.725
Tail surfaces:			
True span, in.	48	24	24
Chord (constant), in.	15.4	7.7	7.7
Angle of incidence, deg	0	0	0
Dihedral, deg	45	45	0
Sweep, deg	0	0	0
Airfoil section	NACA 16-008	NACA 16-008	NACA 16-008
Horizontal area (including fuselage), sq ft	Total projected 7.25	Total projected 1.813	1.283

NATIONAL ADVISORY
COMMITTEE FOR AERONAUTICS

TABLE II.- GENERAL SPECIFICATIONS

Model	Propulsion			Center-of-gravity location (percent chord)		Weight (lb)		Wing loading (lb/sq ft)		Moment of inertia about Y-axis (slug-ft^2)	
	Type rocket	Approximate thrust (lb)	Approximate duration (sec)	Take-off	Burnout	Take-off	Burnout	Take-off	Burnout	Take-off	Burnout
Standard configuration $\delta_f = 0^\circ$	Powder	1200	4.0	15.20	17.40	124.7	97.3	45.7	35.7	8.90	8.50
Standard configuration $\delta_f = 15^\circ$	Powder	1300	3.6	18.58	19.81	127.4	99.9	46.7	36.6	8.30	7.90
Standard configuration $\delta_f = 60^\circ$	Powder	1200	3.8	19.34	18.29	127.1	99.6	46.6	36.6	9.30	8.85
Tail-in-line configuration $\delta_f = 0^\circ$	Powder	1000	3.9	18.86	18.51	125.4	97.9	46.0	35.9	8.30	7.85
Full-scale aircraft	Liquid	600	220	20.00	20.00	1060.0	----	110.0	----	221 (approx.)	----

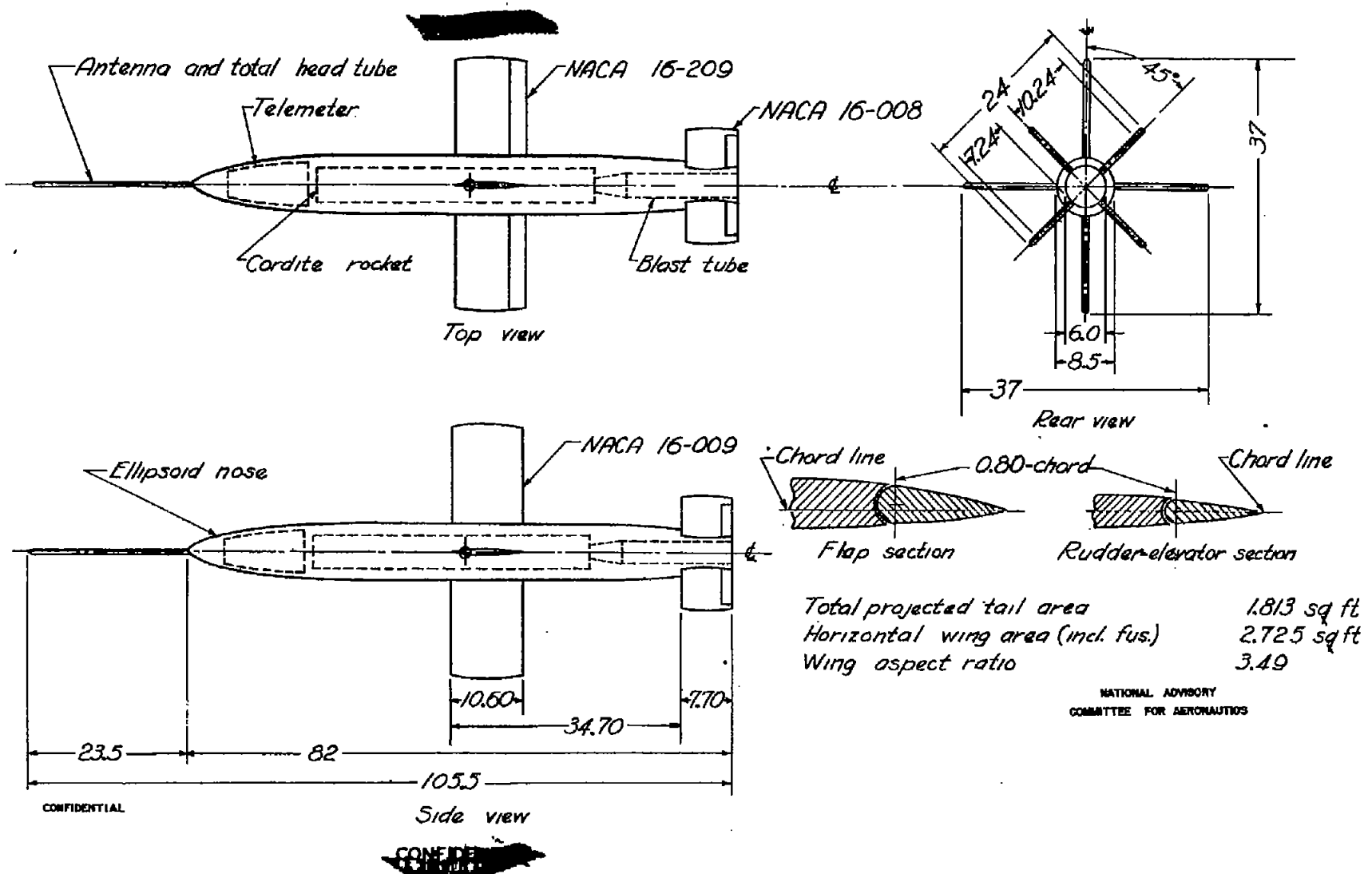

Total projected tail area	1.813 sq ft
Horizontal wing area (incl. fus.)	2.725 sq ft
Wing aspect ratio	3.49

NATIONAL ADVISORY
COMMITTEE FOR AERONAUTICS

CONFIDENTIAL

CONFIDENTIAL

Figure 1.- General arrangement of 0.5-scale model of Lark Pilotless Aircraft; all dimensions in inches; all wing and tail tips are solids of revolution.

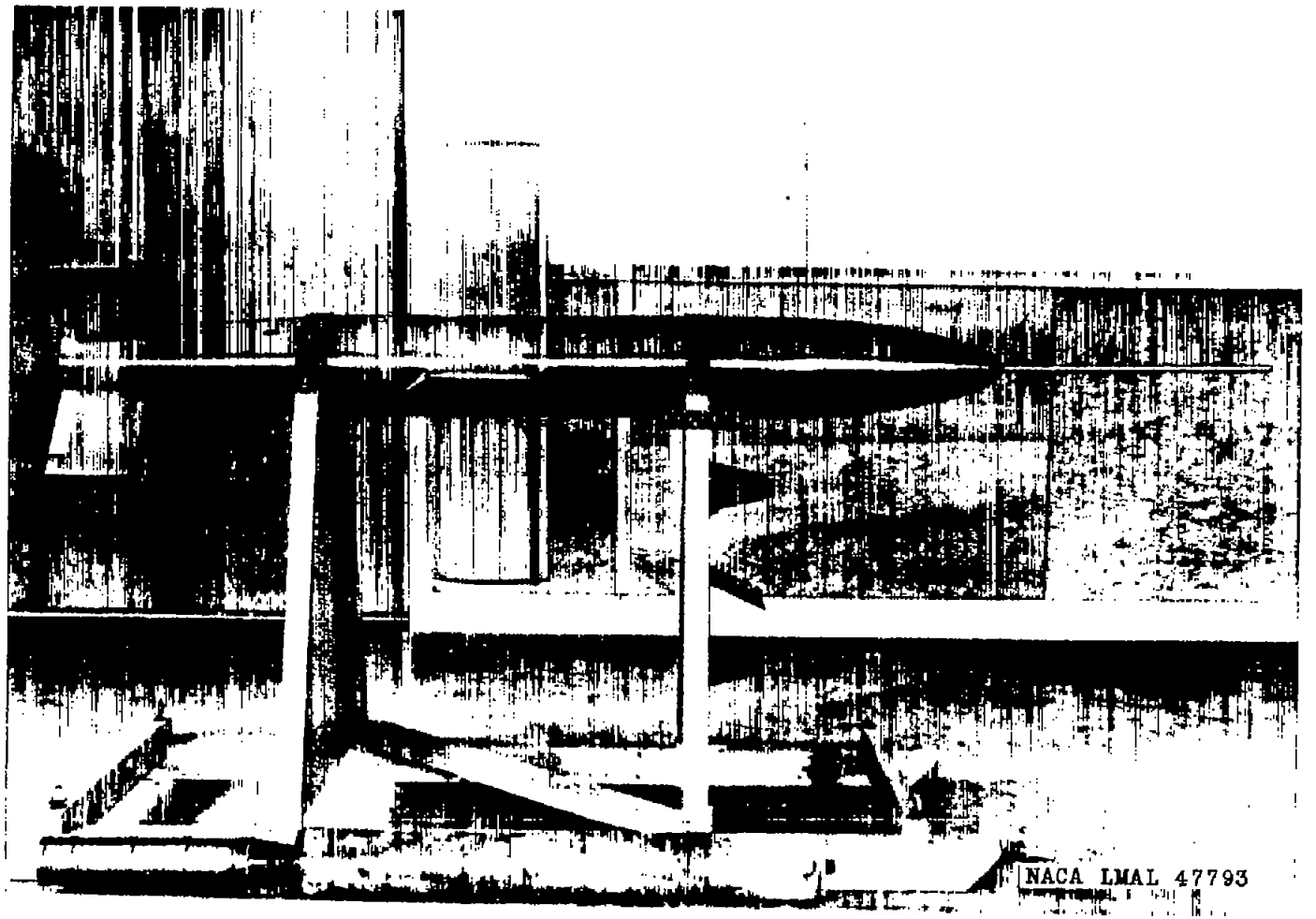

Figure 2.- Photographs of 0.5-scale standard configuration model Lark and rocket motor with blast tube.

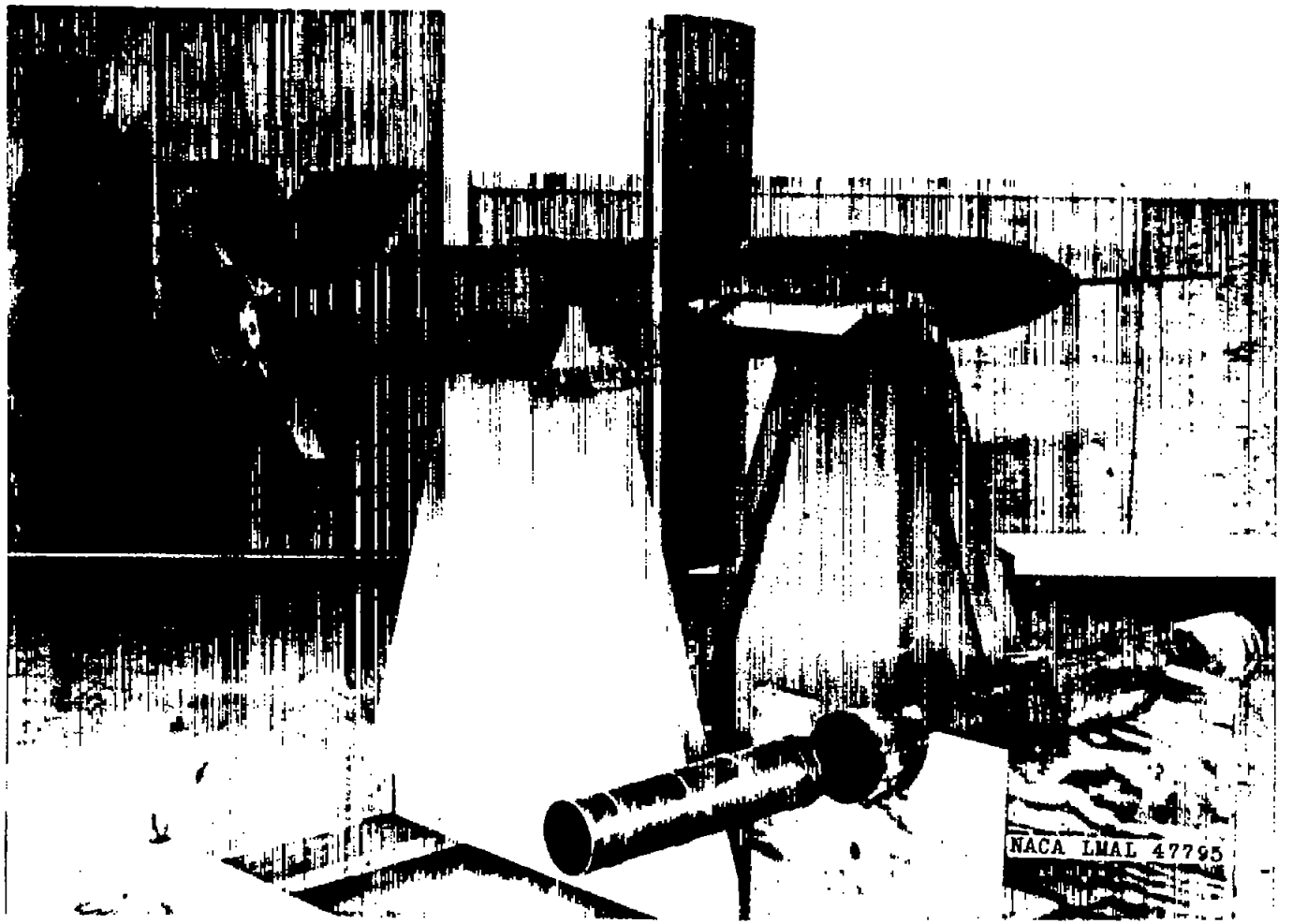

Figure 2.- Concluded.

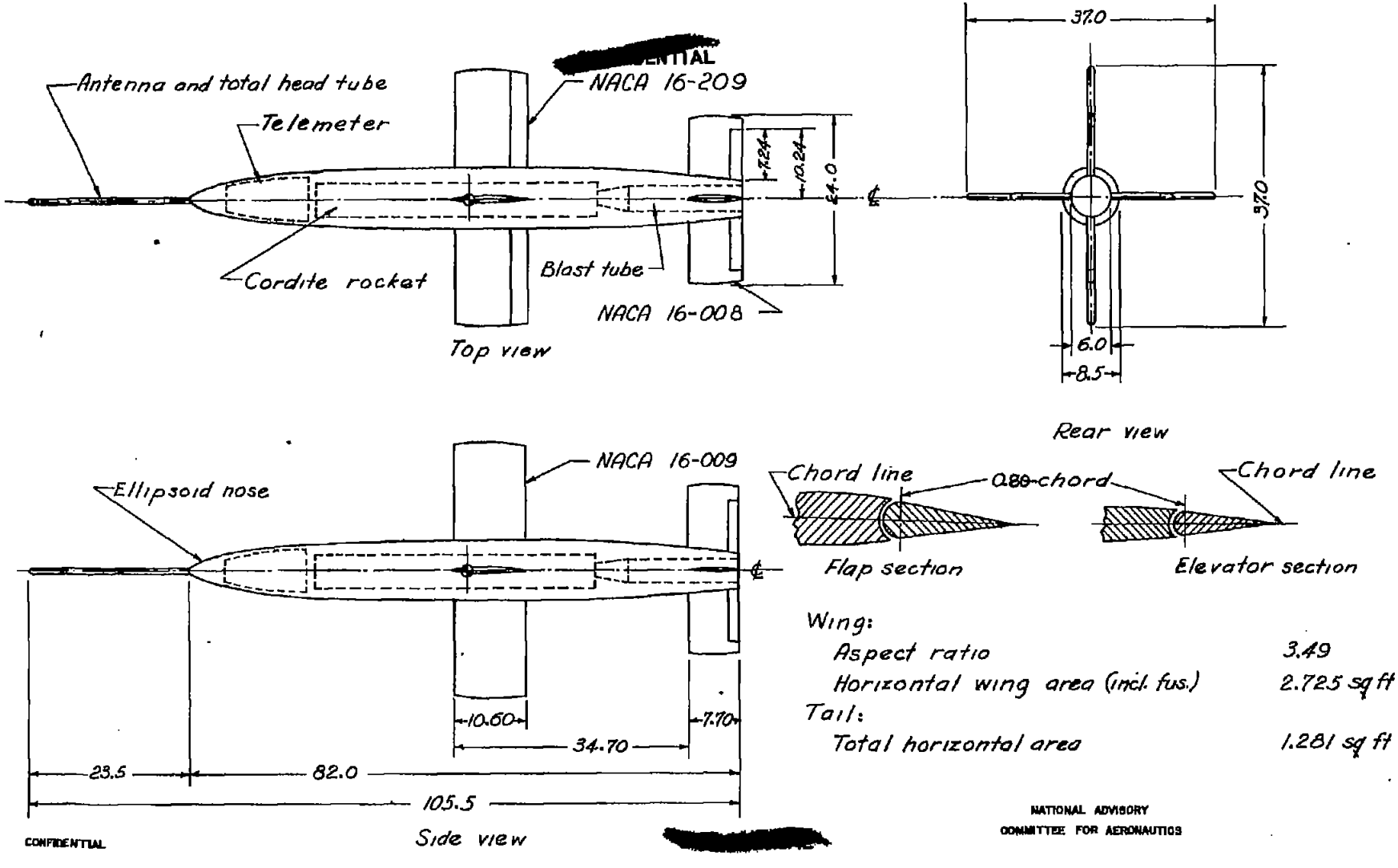

Figure 3.-General arrangement of 0.5-scale model of Lark Pilotless Aircraft with tail in line with wing; all dimensions in inches; all wing and tail tips are solids of revolution.

Figure 4.- Photograph of tail-in-line model with rocket motor and blast tube.

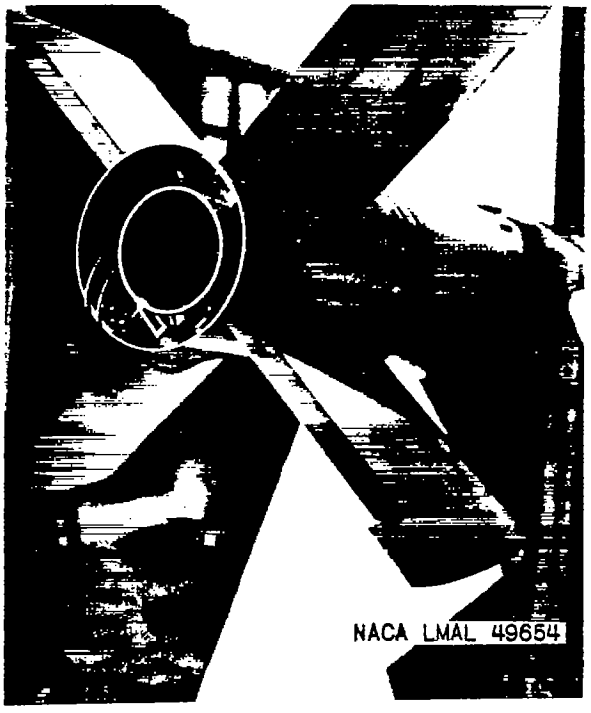

Figure 5.- Tail-view photograph of a 0.5-scale model Lark.

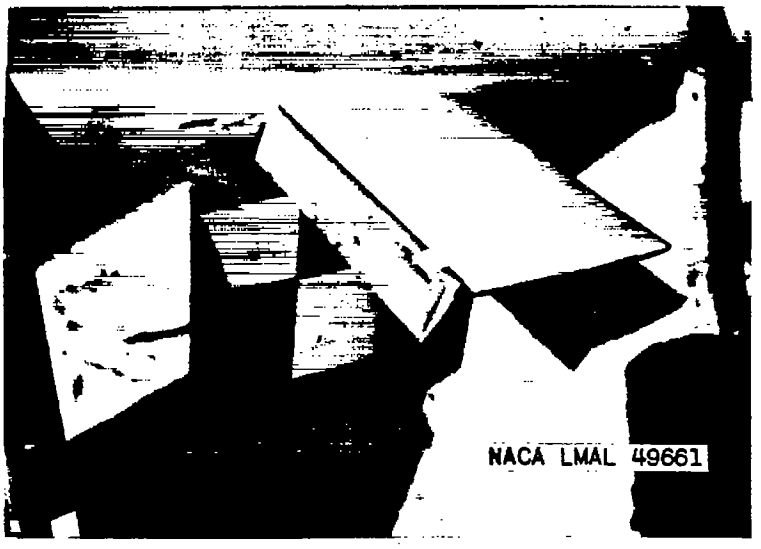

Figure 6.- Horizontal wing flap deflected 60° on standard configuration model.

CONFIDENTIAL

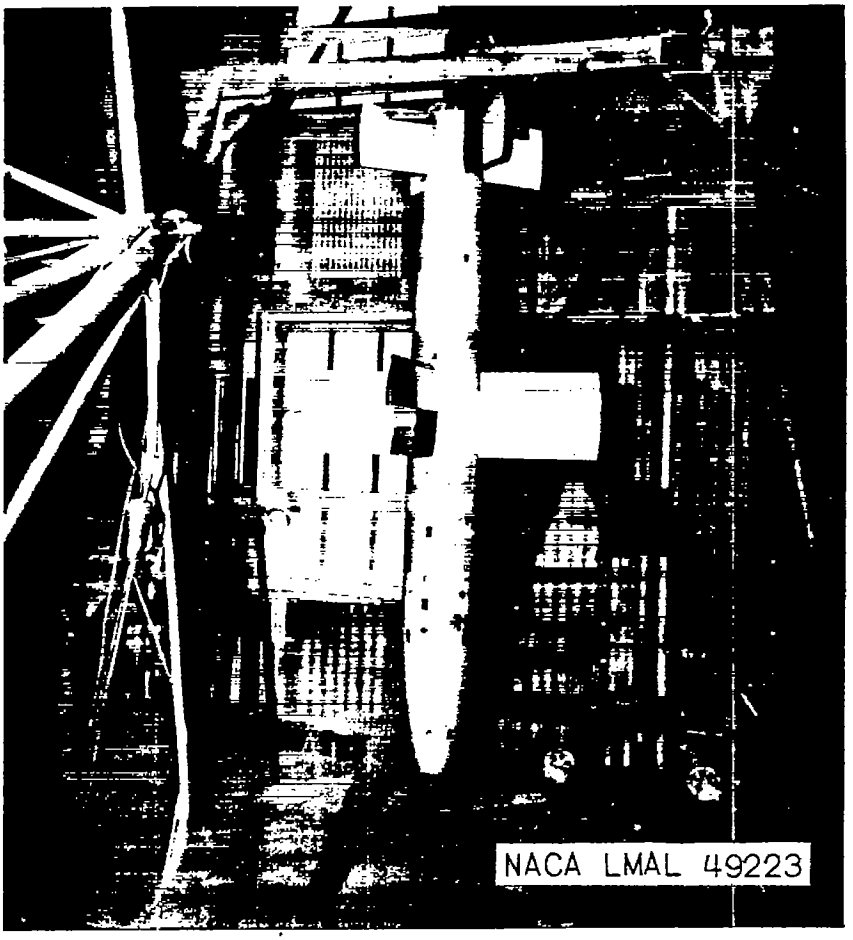

Figure 7.- Model mounted on swinging rig for determining the moment of inertia.

CONFIDENTIAL

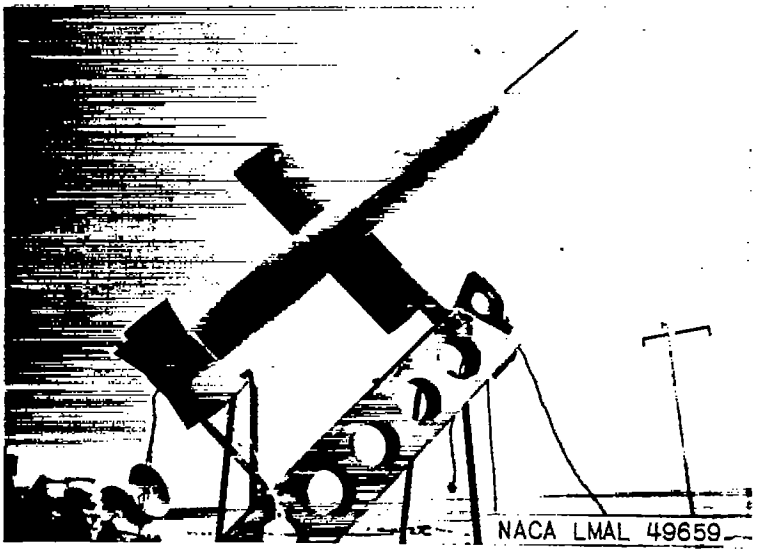

(a) Standard configuration model; $_f = 60^\circ$.

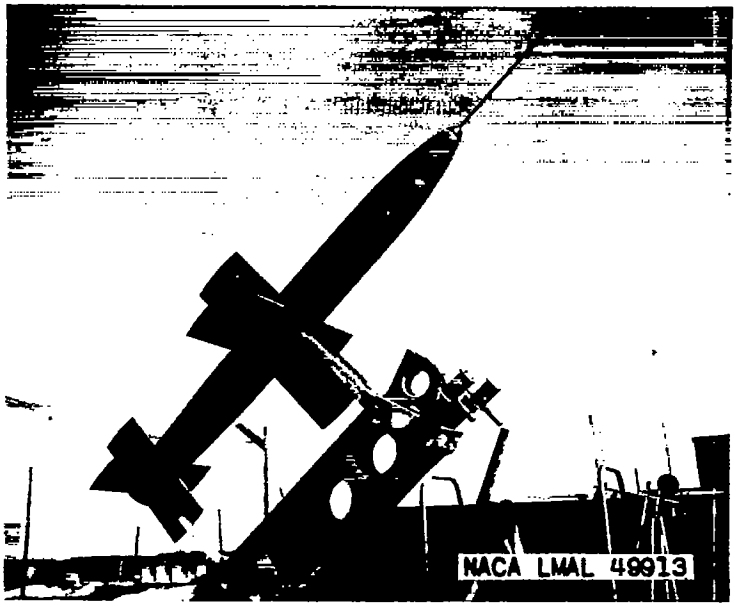

(b) Tail-in-line model; $_f = 0^\circ$.

Figure 8.- Model Larks on launcher.

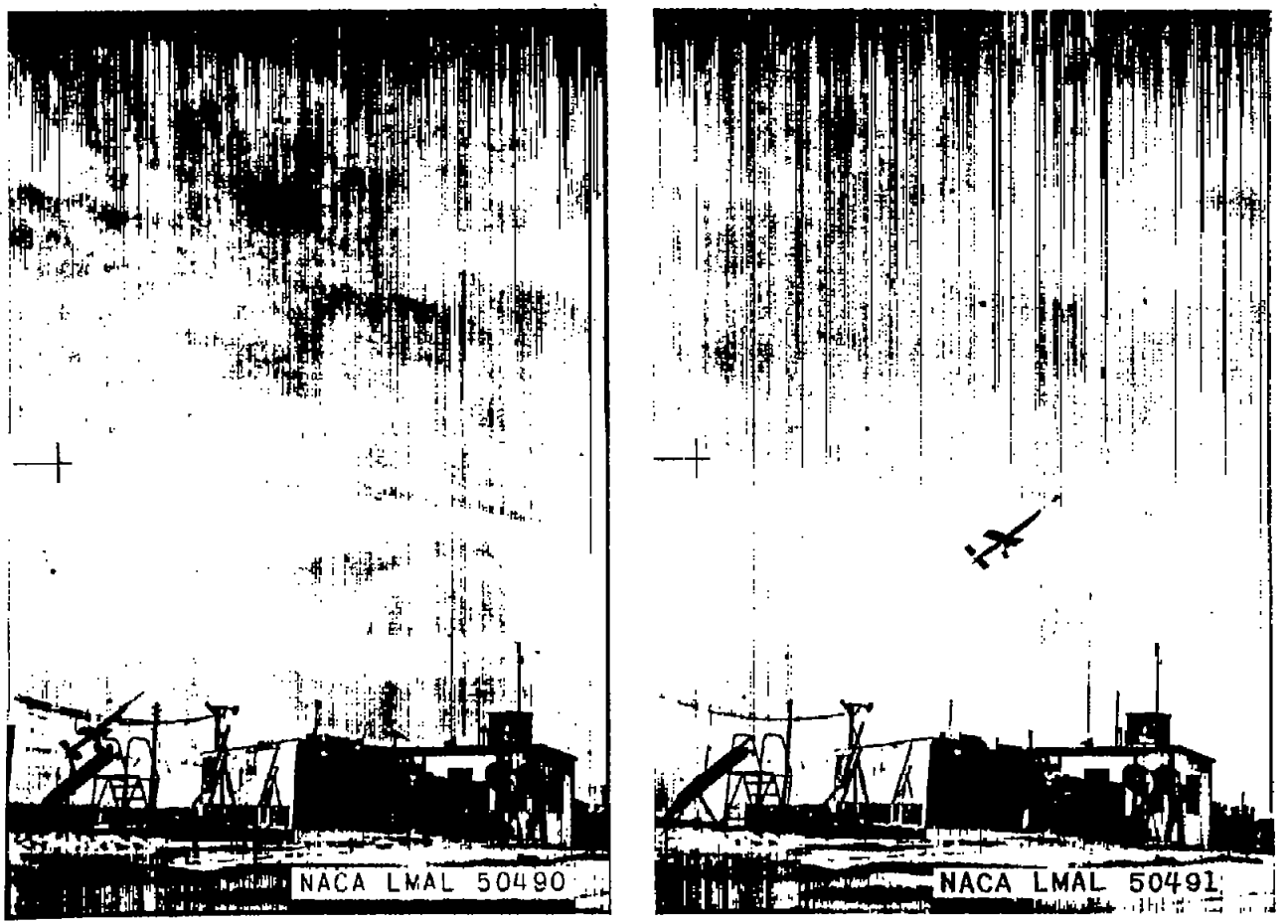

Figure 9.- Launching of 0.5-scale model Lark; standard configuration; $\alpha_f = 60^\circ$.

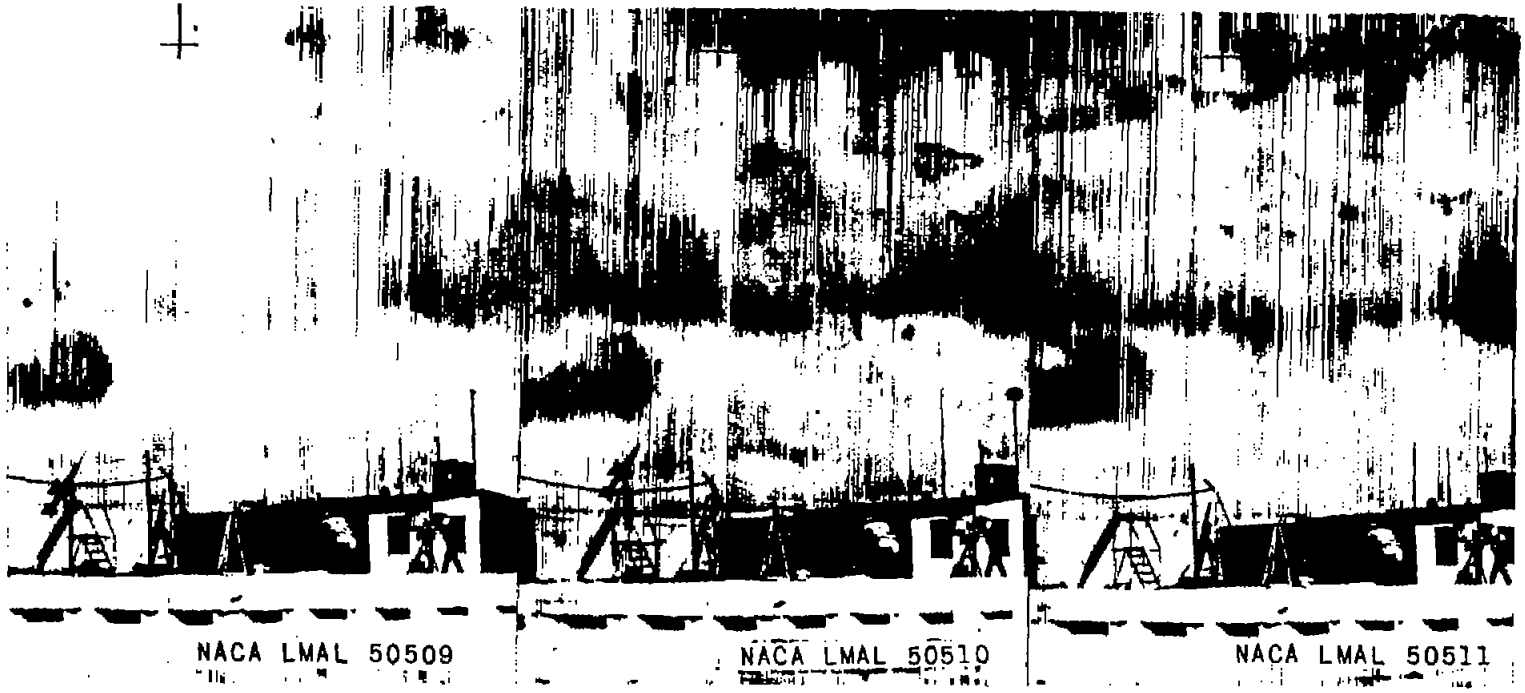

Figure 10.- Launching of 0.5-scale model Lark; configuration with tail in line with wings; $i_f = 0^\circ$.

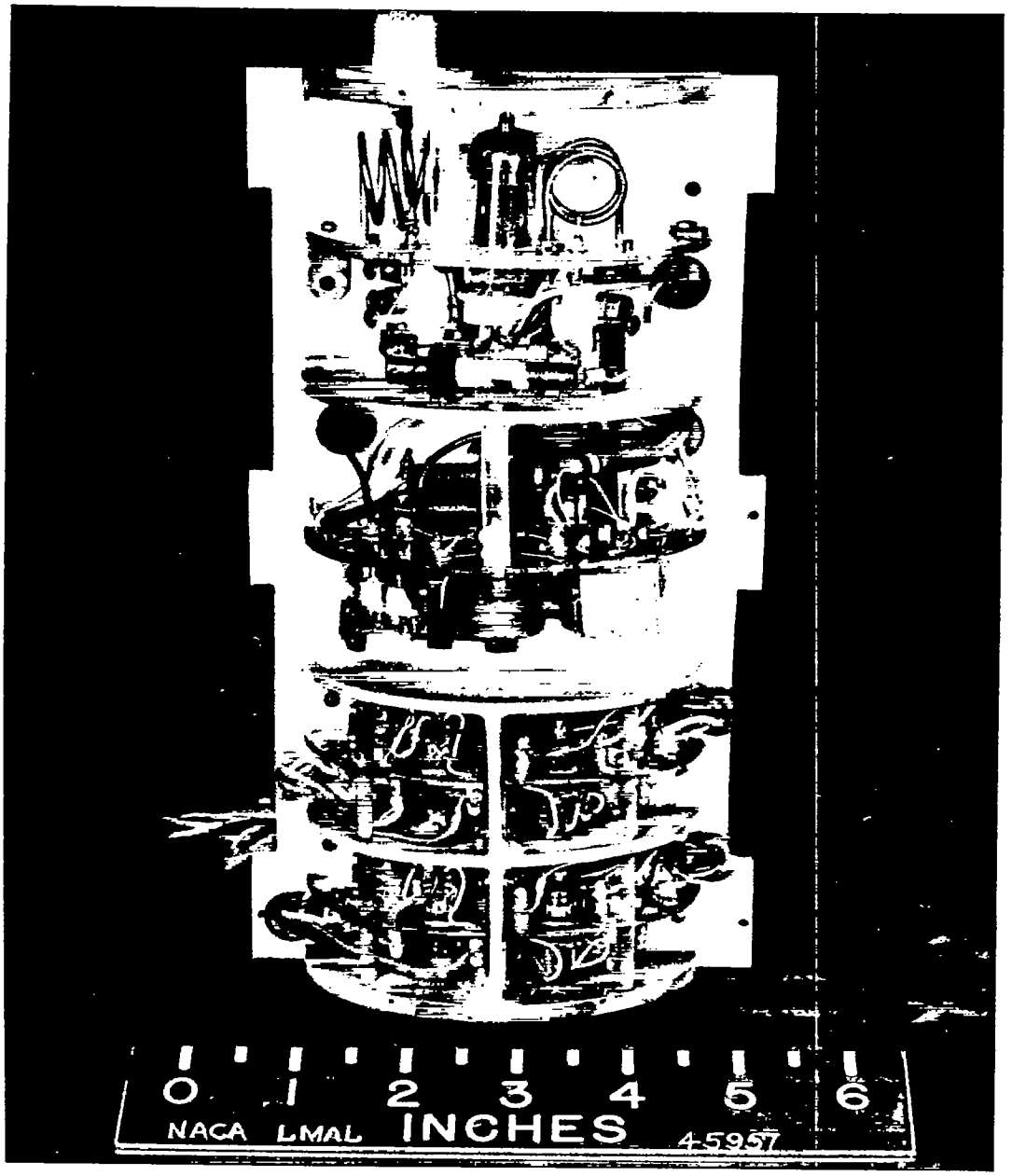

Figure 11.- Photograph of the radio-transmitter part of the telemeter system.

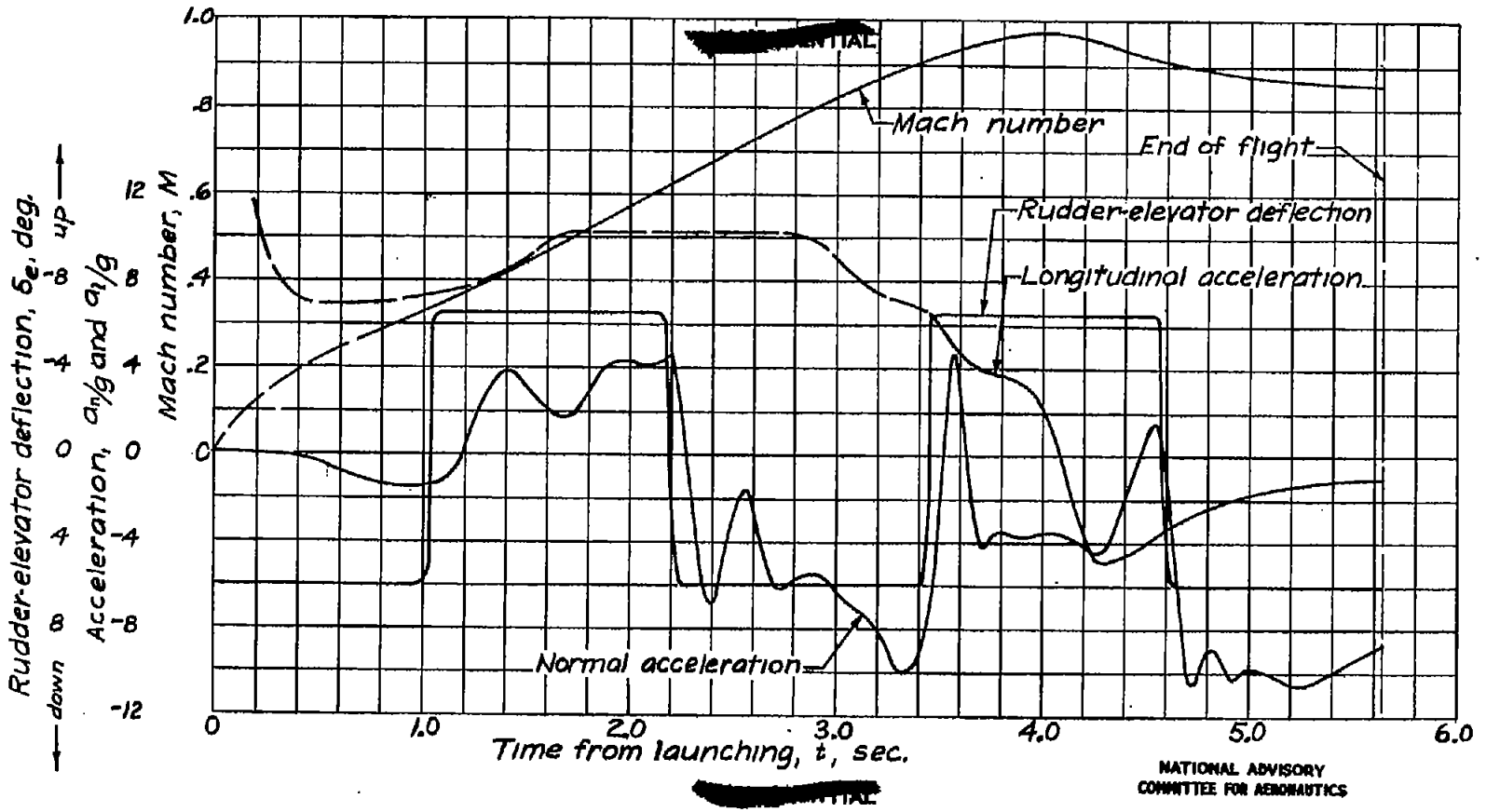

Figure 12.-Variation of Mach number, rudder-elevator deflection, and normal and longitudinal accelerations with time. 0.5-scale model Lark of standard configuration; $\delta_f = 0°$.

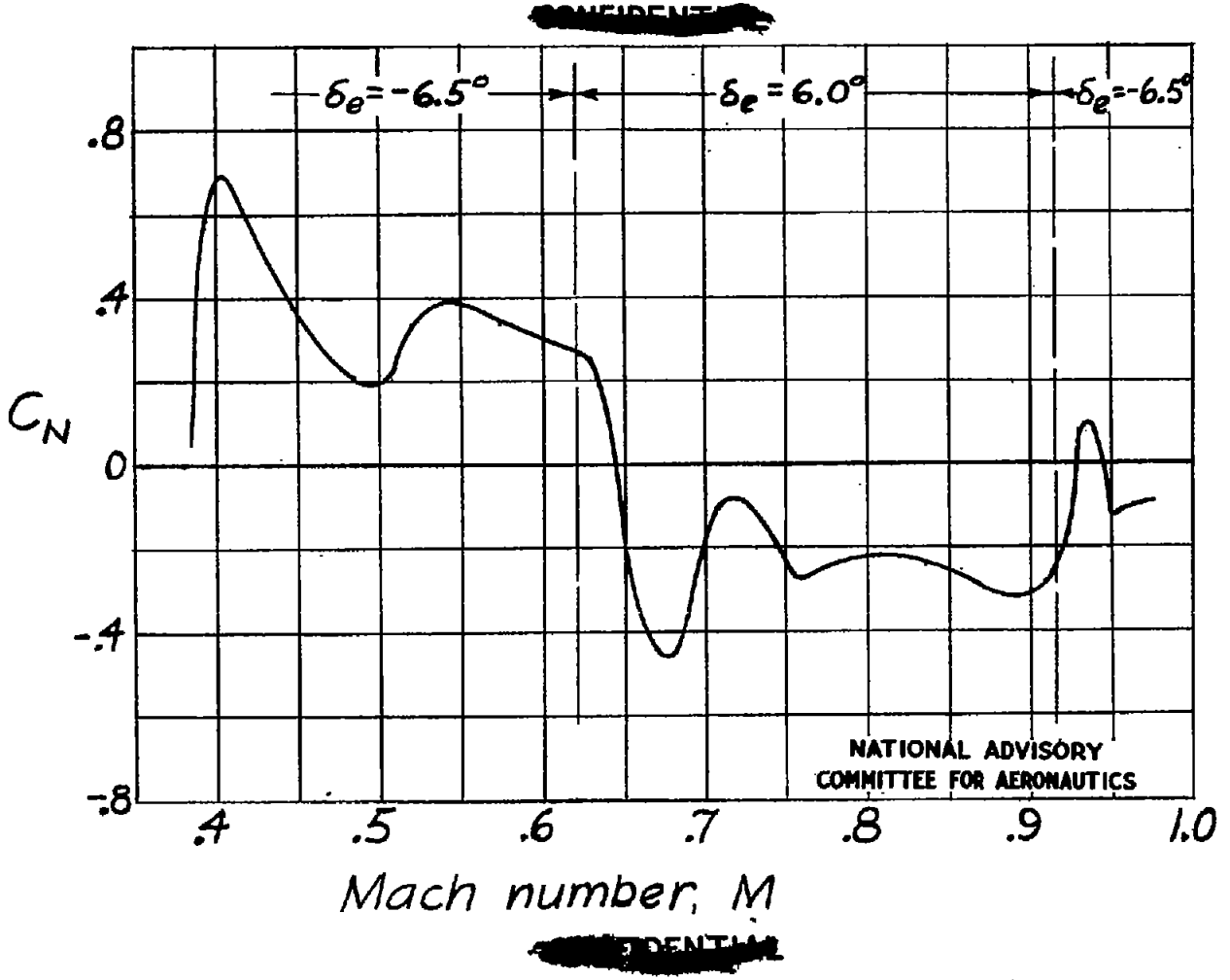

Figure 13.-Variation of normal-force coefficient with Mach number for the power-on portion of the flight. Model of standard configuration; $\delta_f = 0°$

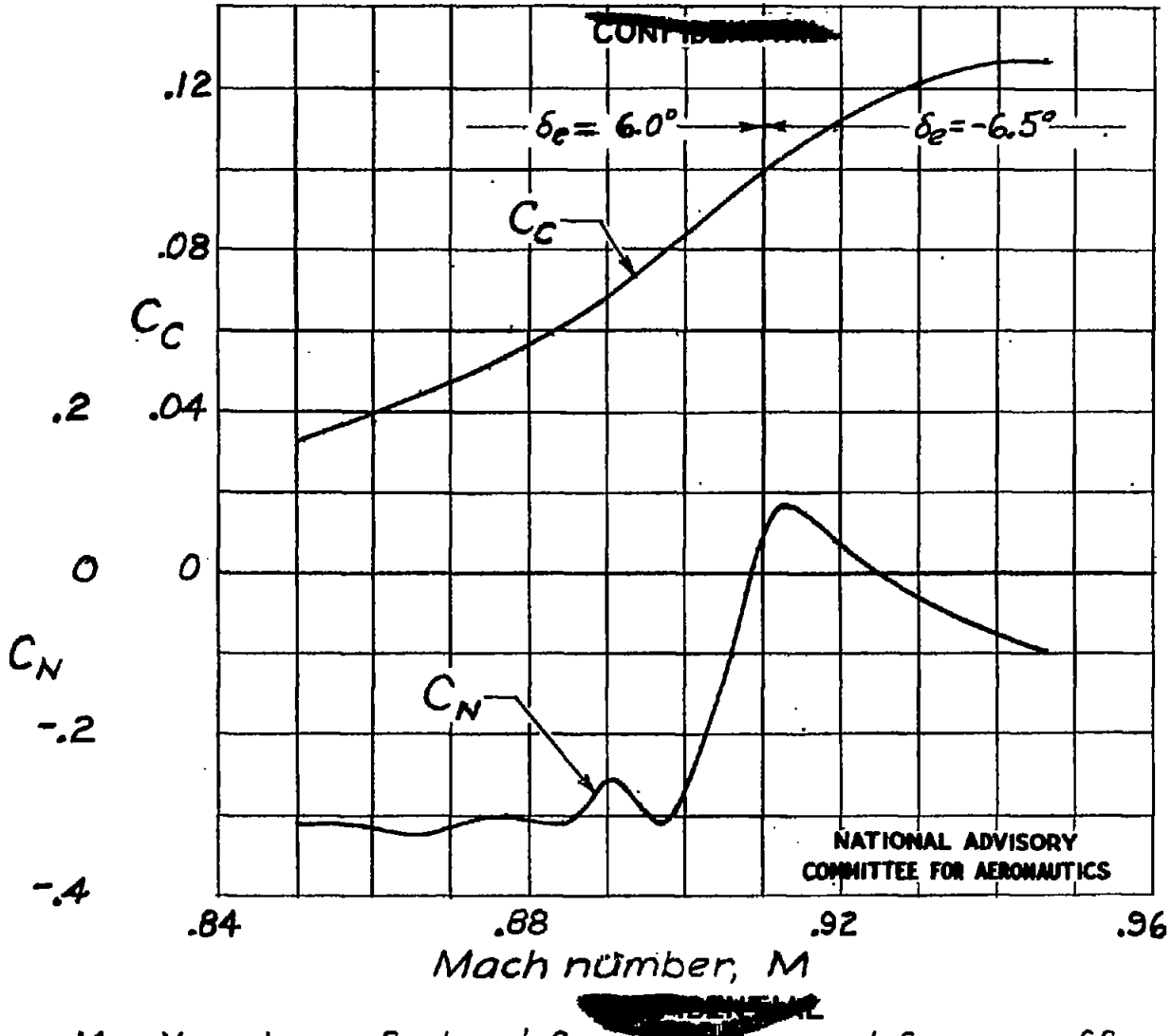

Figure 14. - Variation of chord-force and normal-force coefficients with Mach number for the power-off portion of the flight. Model of standard configuration; $\delta_f = 0°$

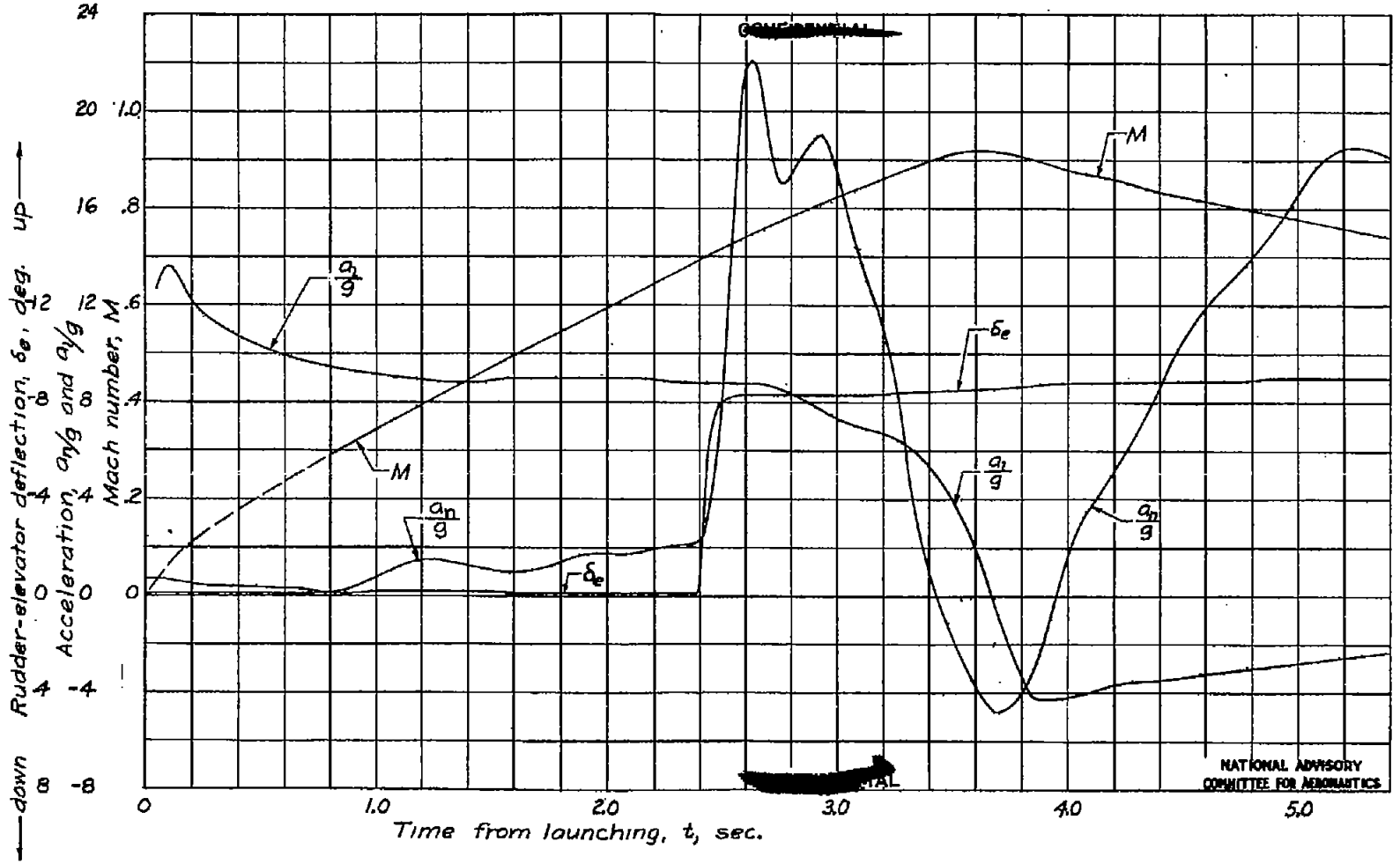

Figure 15.- Variation of Mach number, rudder-elevator deflection, and normal and longitudinal accelerations with time. 0.5-scale model Lark of standard configuration; $\delta_f = 15°$

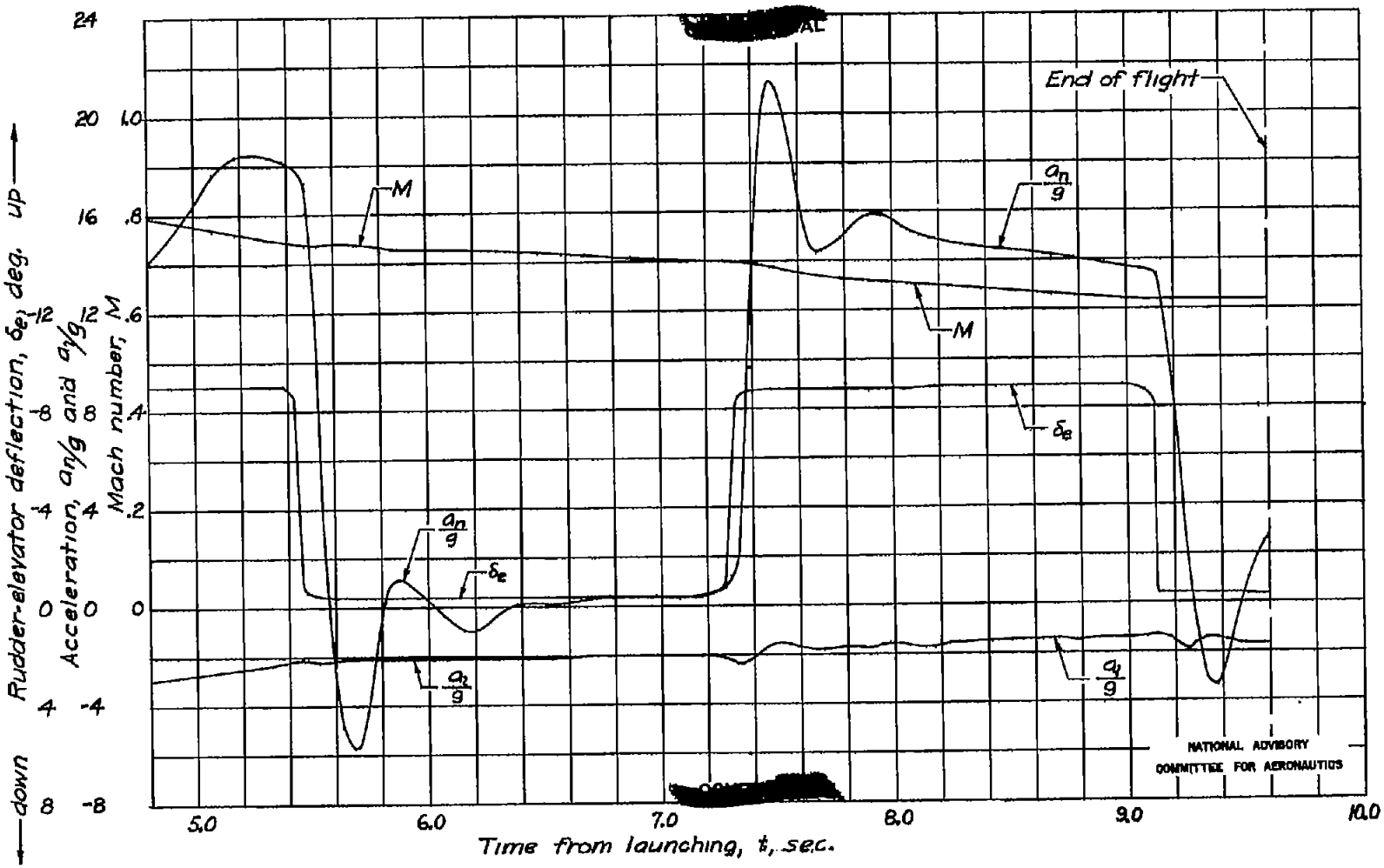

Figure 15.- Concluded.

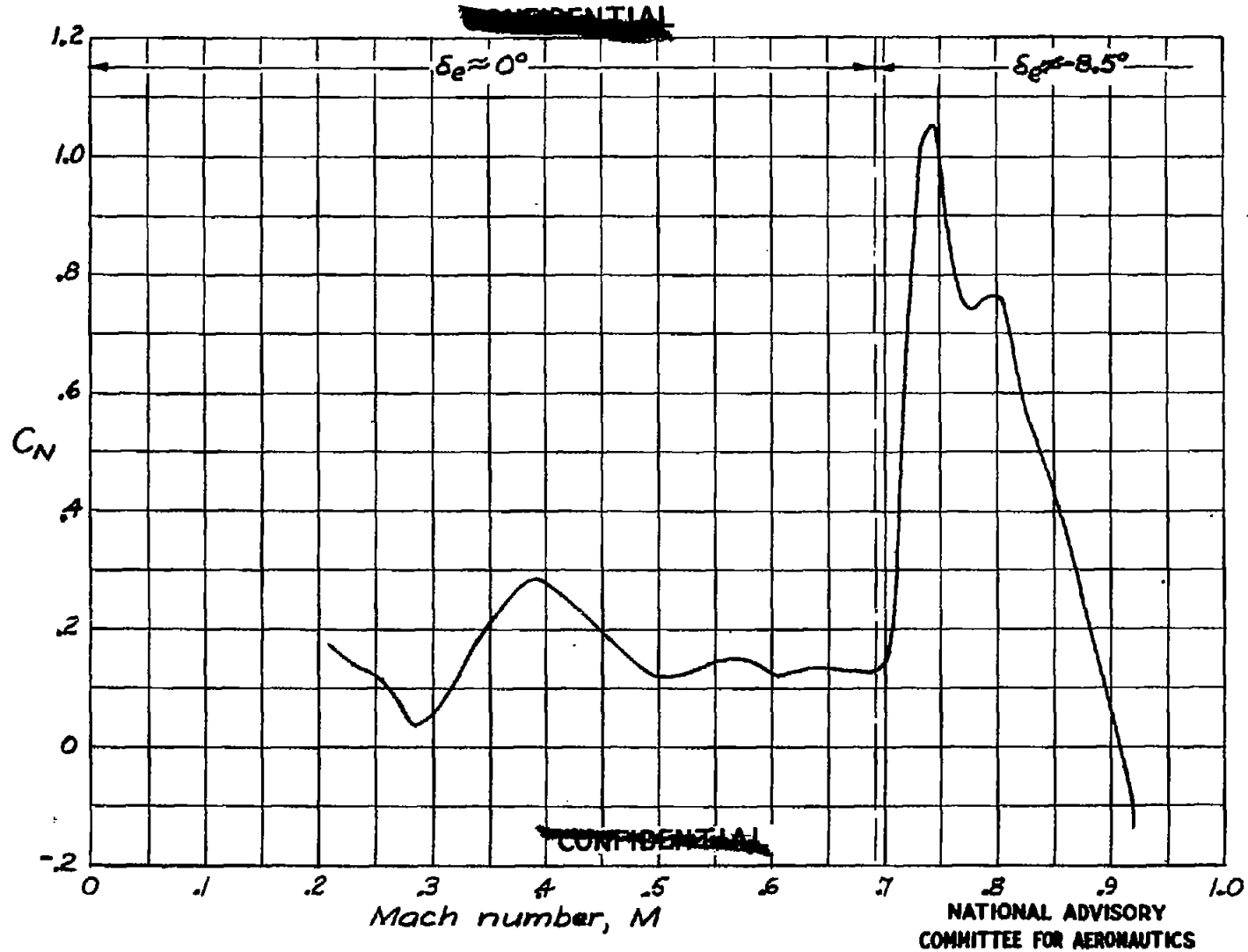

Figure 16.-Variation of normal-force coefficient with Mach number for the power-on portion of the flight. Model of standard configuration; δ_f=15°.

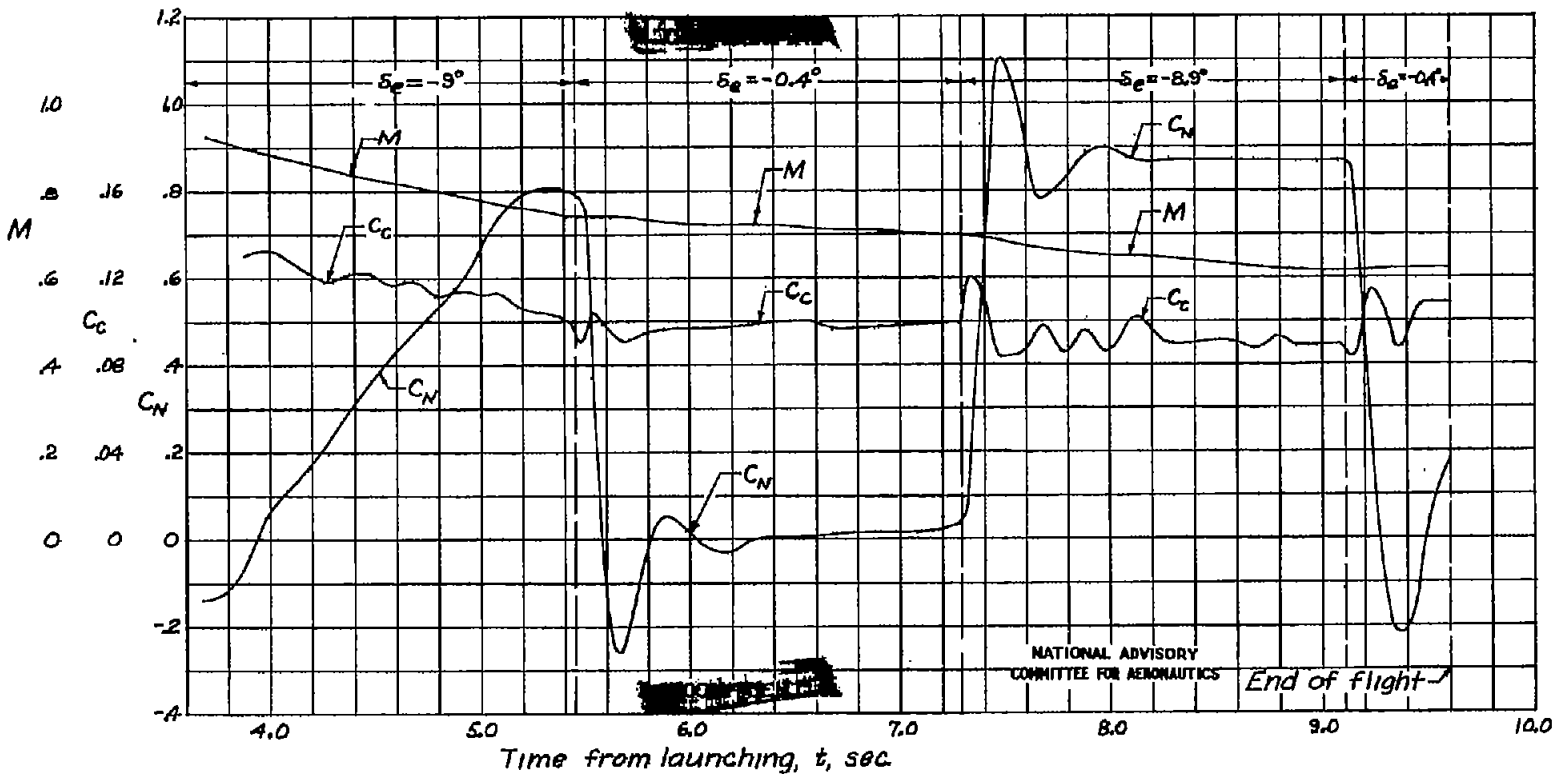

Figure 17.- Variation of Mach number and chord-force and normal-force coefficients with time for the power-off portion of the flight. Model of standard configuration; δ_f = 15°.

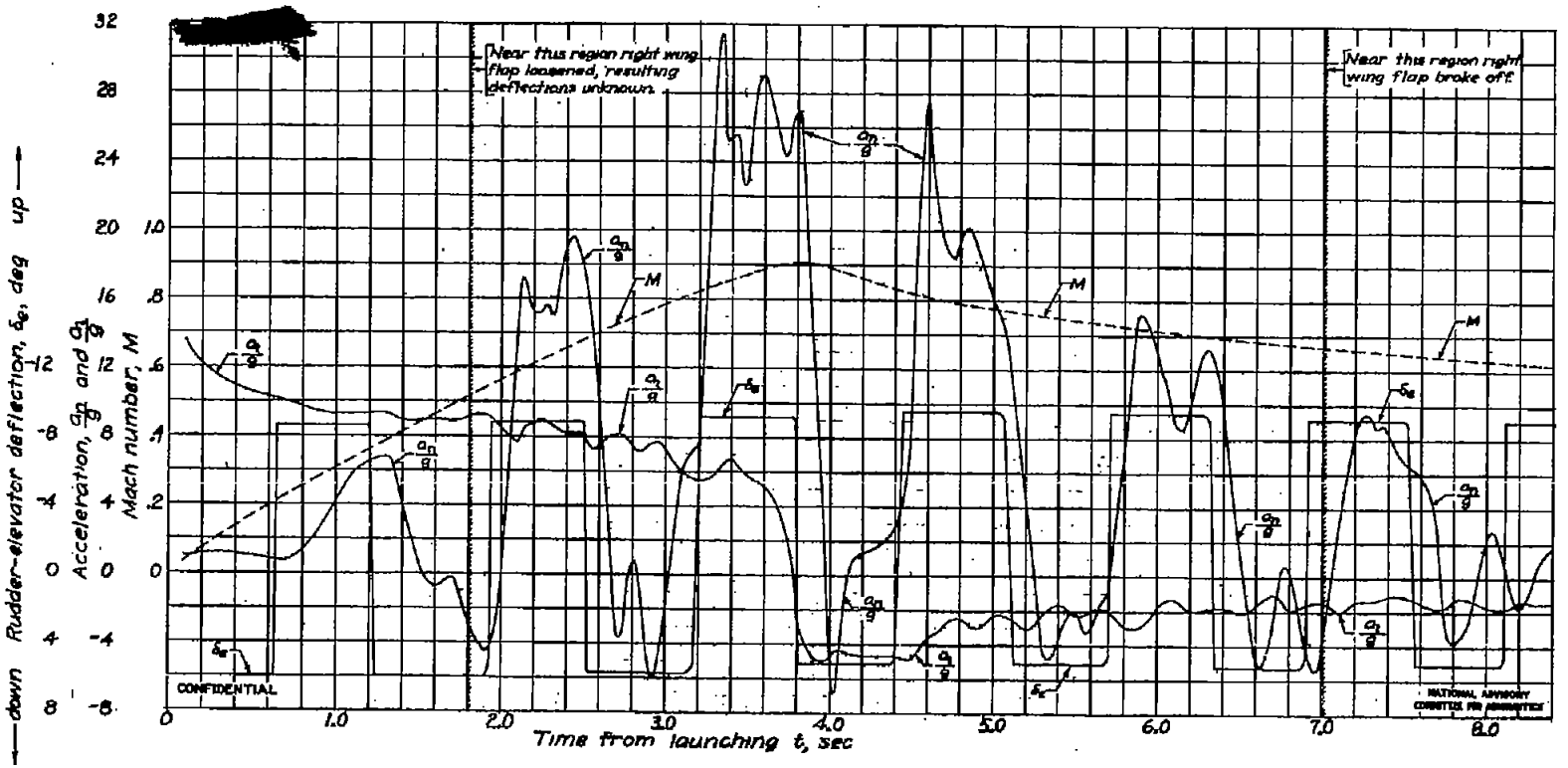

Figure 18.- Variation of Mach number, rudder-elevator deflection, and normal and longitudinal accelerations with time. 0.5-scale model Lark of standard configuration; $\delta_f = 60°$.

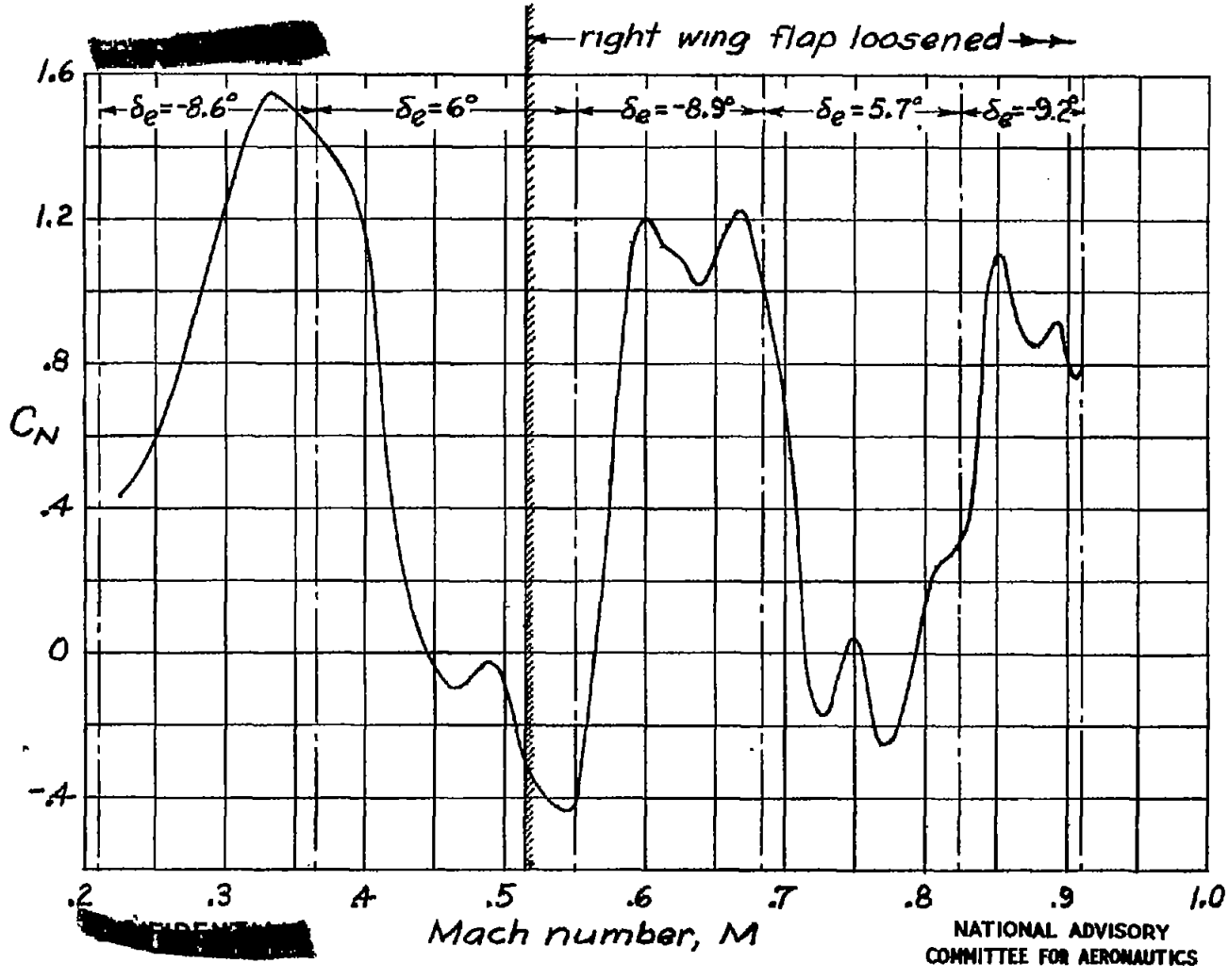

Figure 19.- Variation of normal-force coefficient with Mach number for the power-on part of the flight. Model of standard configuration; $\delta_f \approx 60°$.

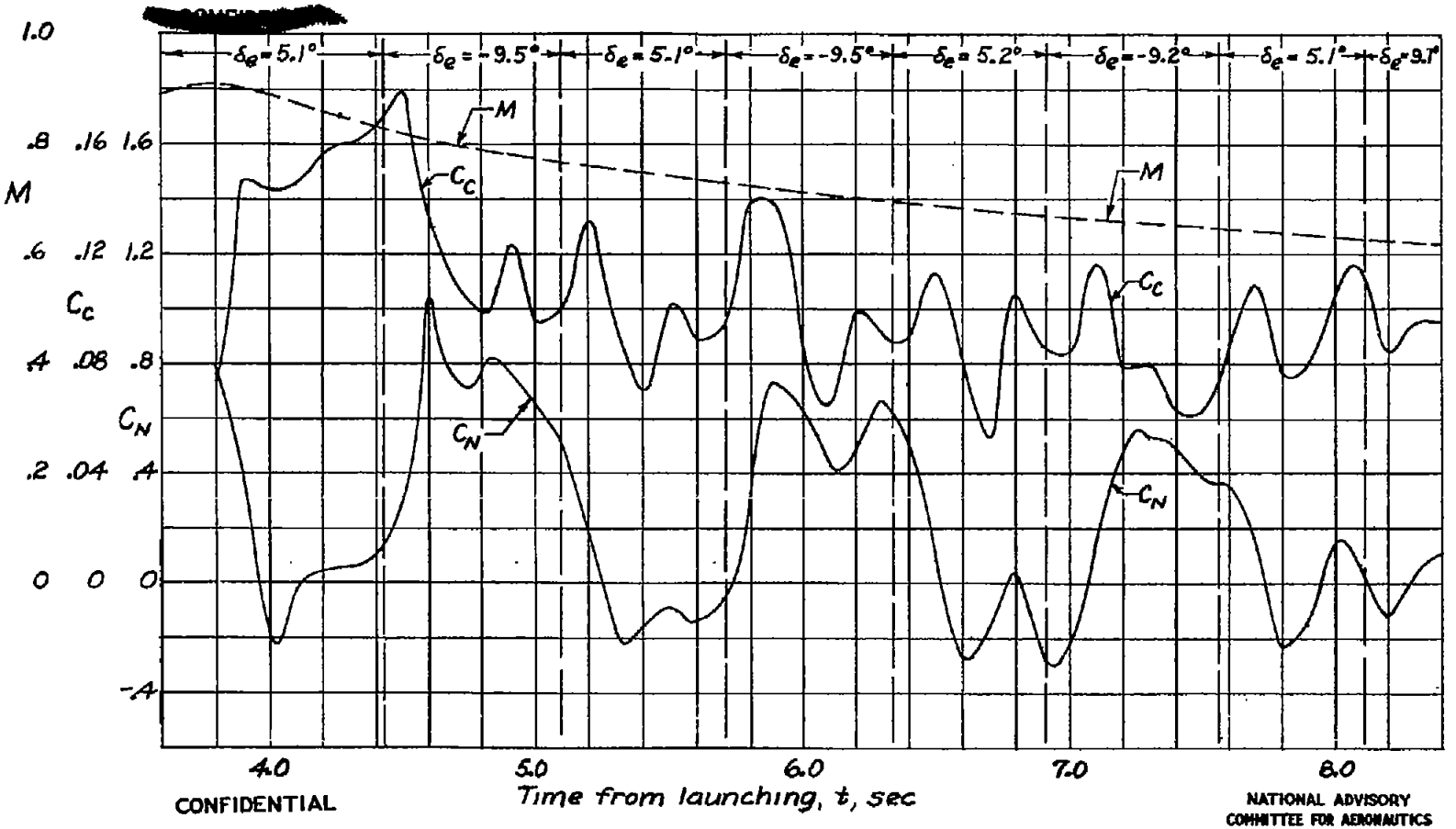

Figure 20.- Variation of Mach number and chord-force and normal-force coefficients with time for the power-off part of the flight. Model of standard configuration; $\delta_f \approx 60°$.

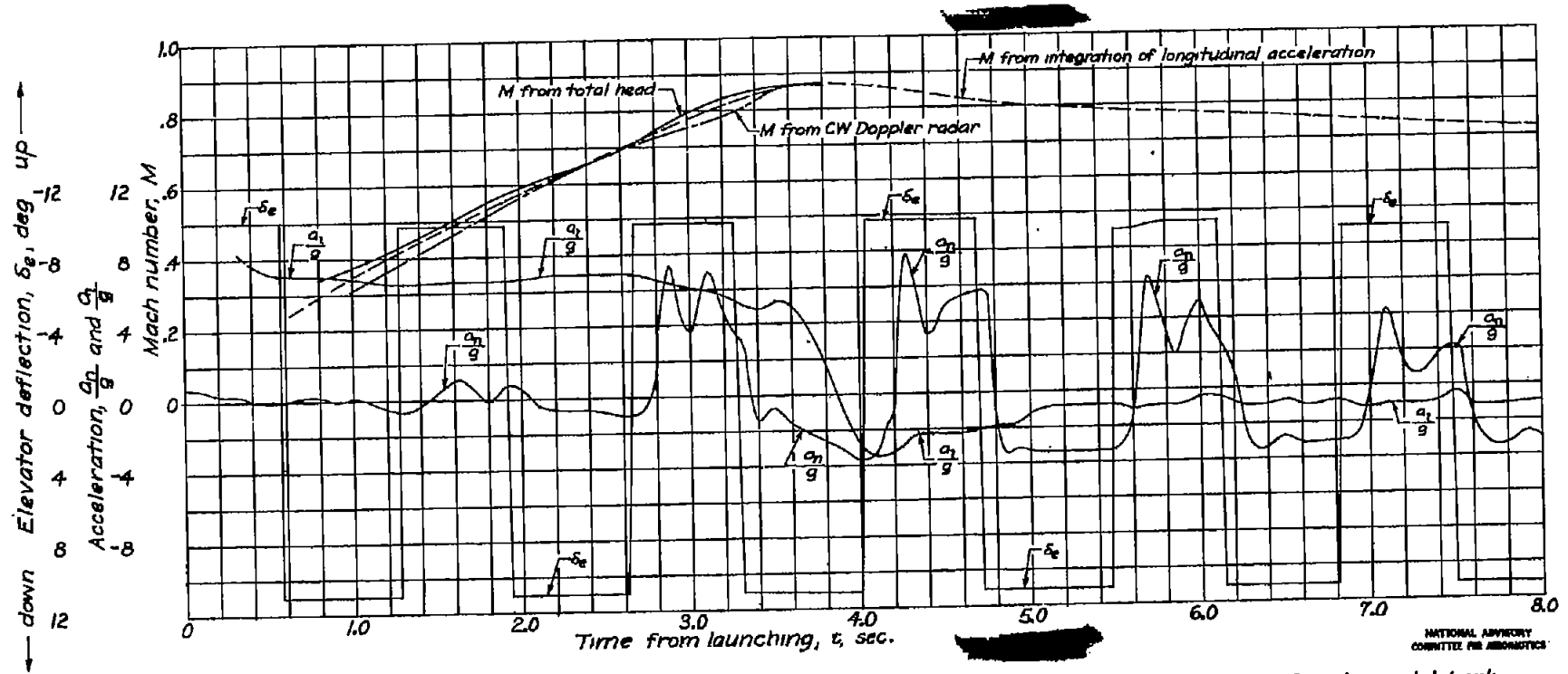

Figure 21.- Variation of Mach number, elevator deflection, and normal and longitudinal accelerations with time. 0.5-scale model Lark with tail in line with wings; $\delta_t = 0°$

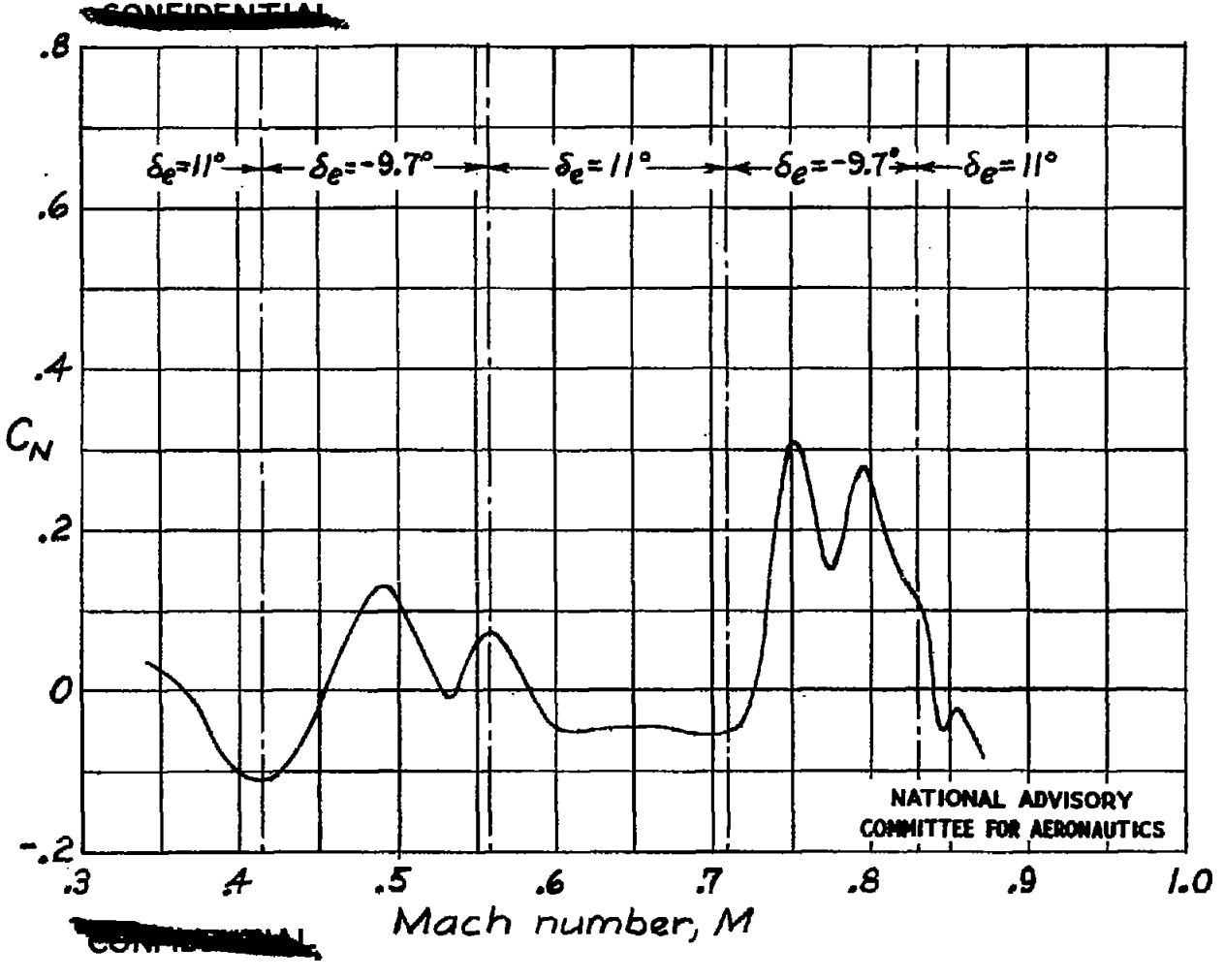

Figure 22.- Variation of normal-force coefficient with Mach number for the power-on part of the flight. Model with tail in line with wings; $\delta_f = 0°$.

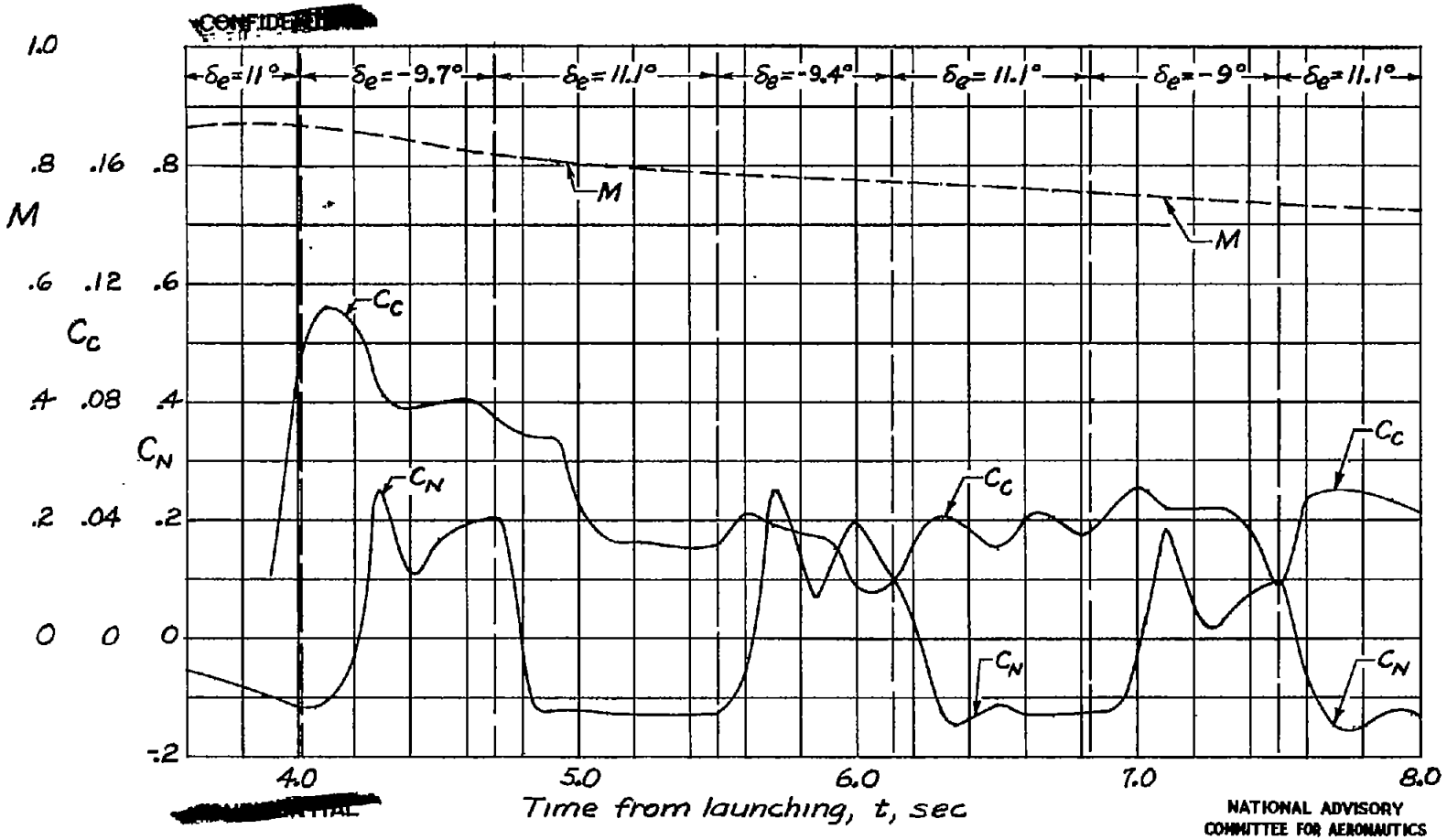

Figure 23.-Variation of Mach number and chord-force and normal-force coefficients with time for the power-off part of the flight. Model with tail in line with wings; $\delta_r = 0°$.

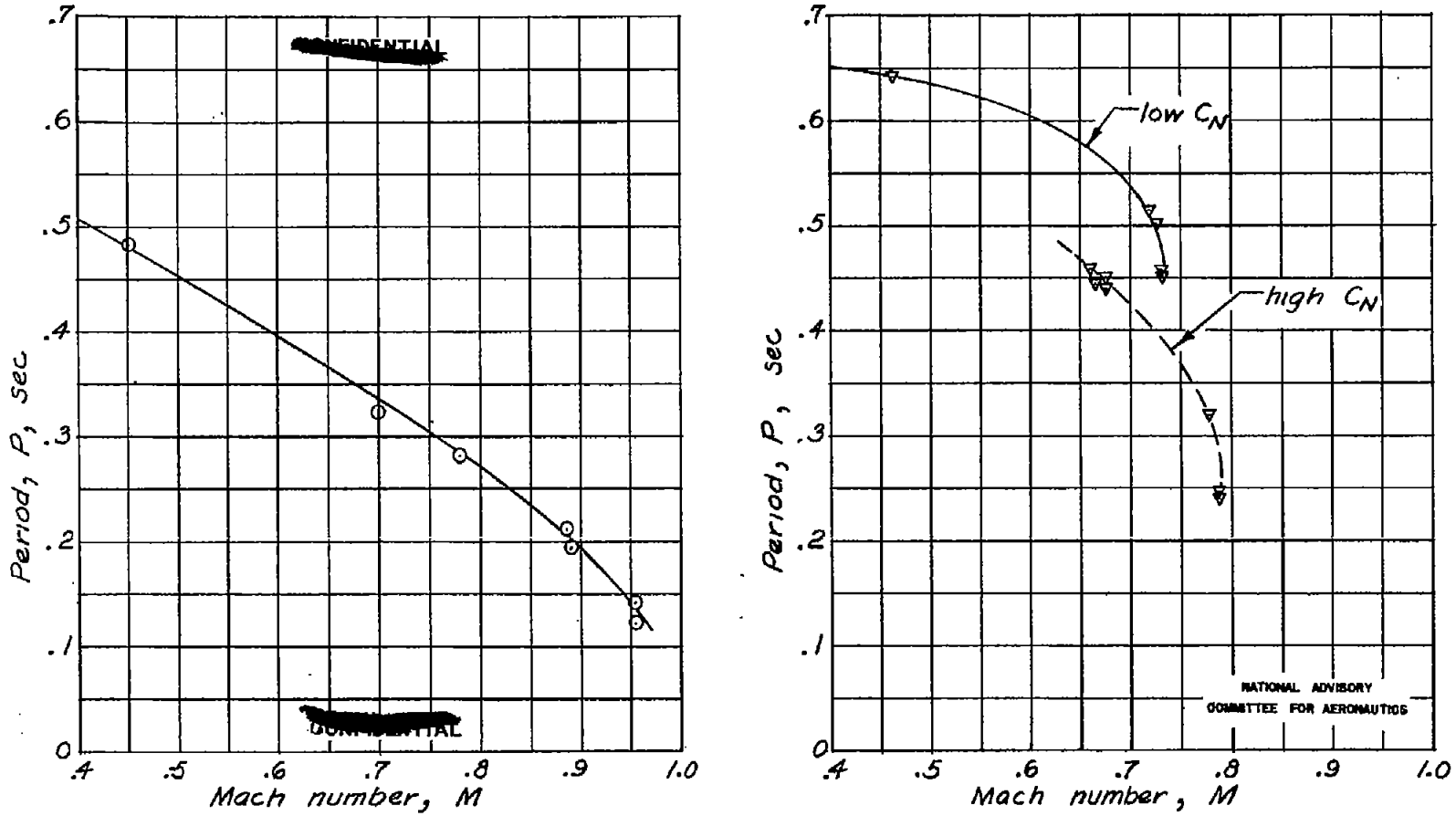

(a) Standard configuration; $\delta_f = 0°$

(b) Standard configuration; $\delta_f = 15°$

Figure 24.- Variation of period of the short-period oscillations with Mach number.

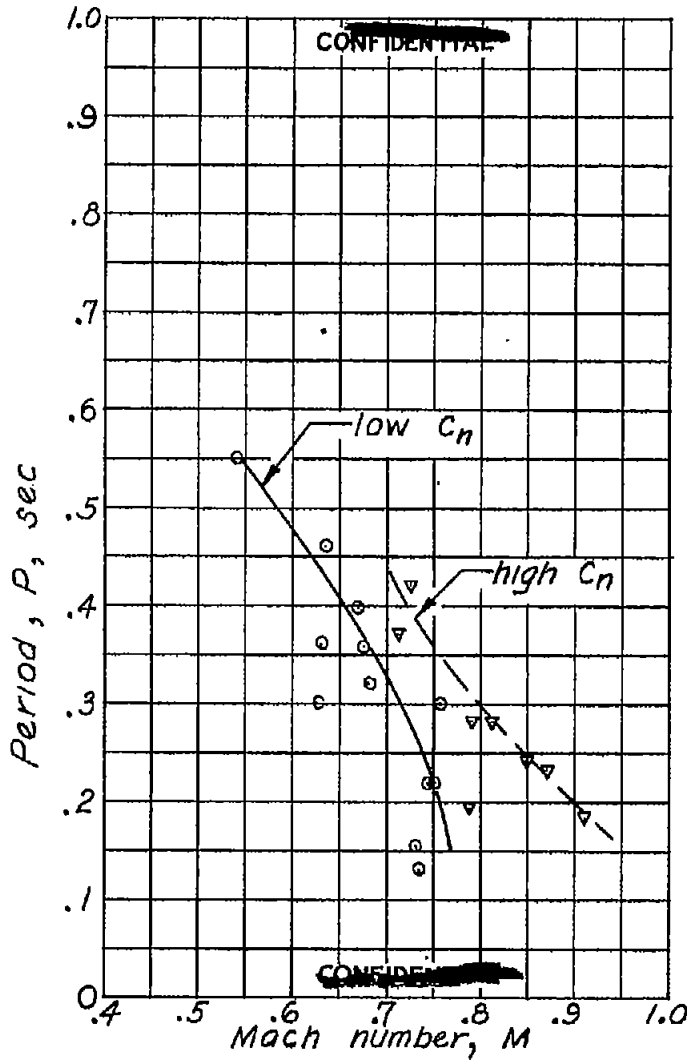

(c) Standard configuration; $\delta_f \approx 60°$

Figure 24. - Concluded.

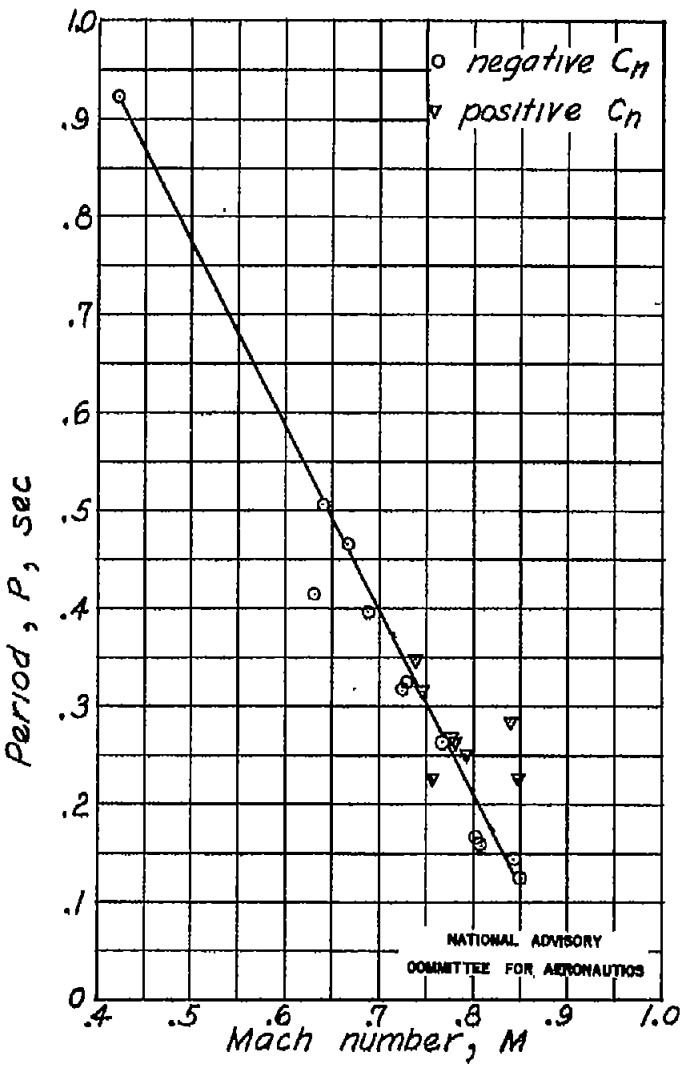

(d) Tail in line; $\delta_f = 0°$

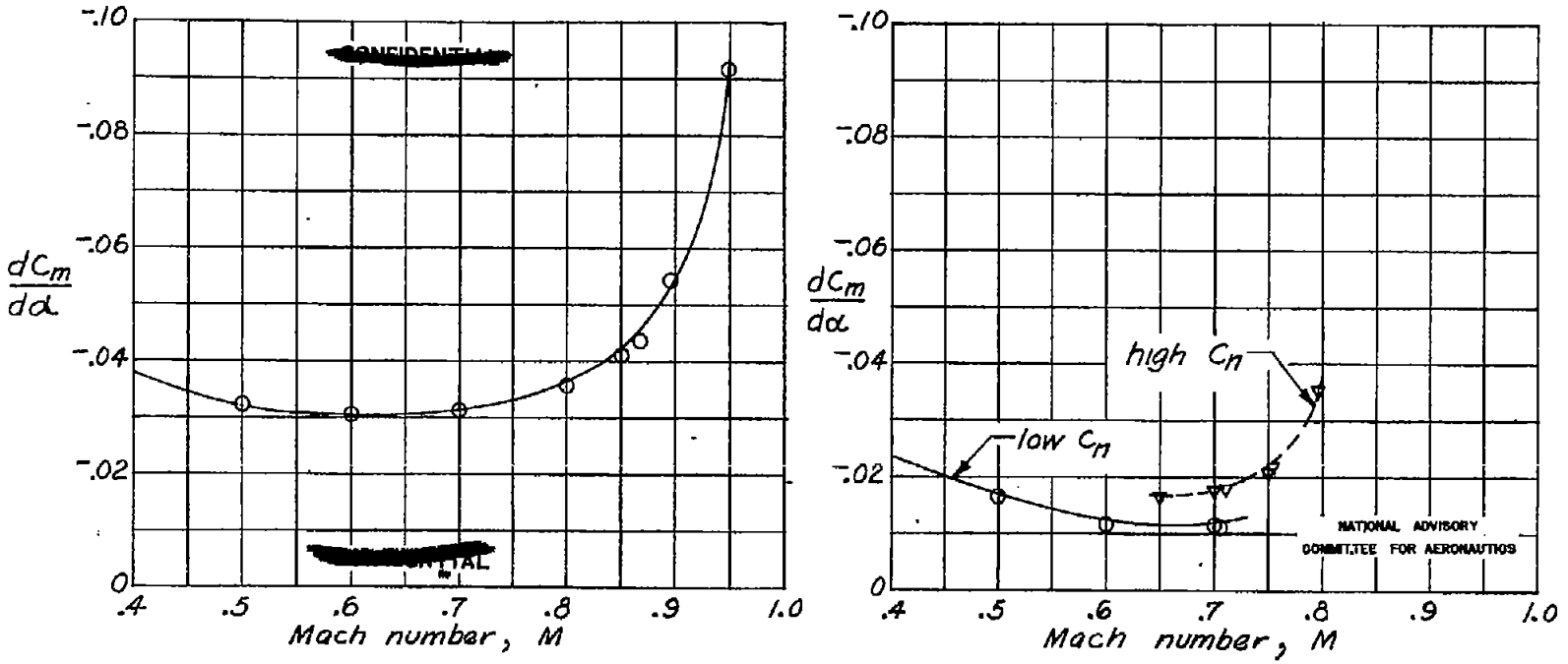

(a) Standard configuration ; $\delta_f = 0°$

(b) Standard configuration ; $\delta_f = 15°$

Figure 25. - Variation of the static longitudinal stability with Mach number.

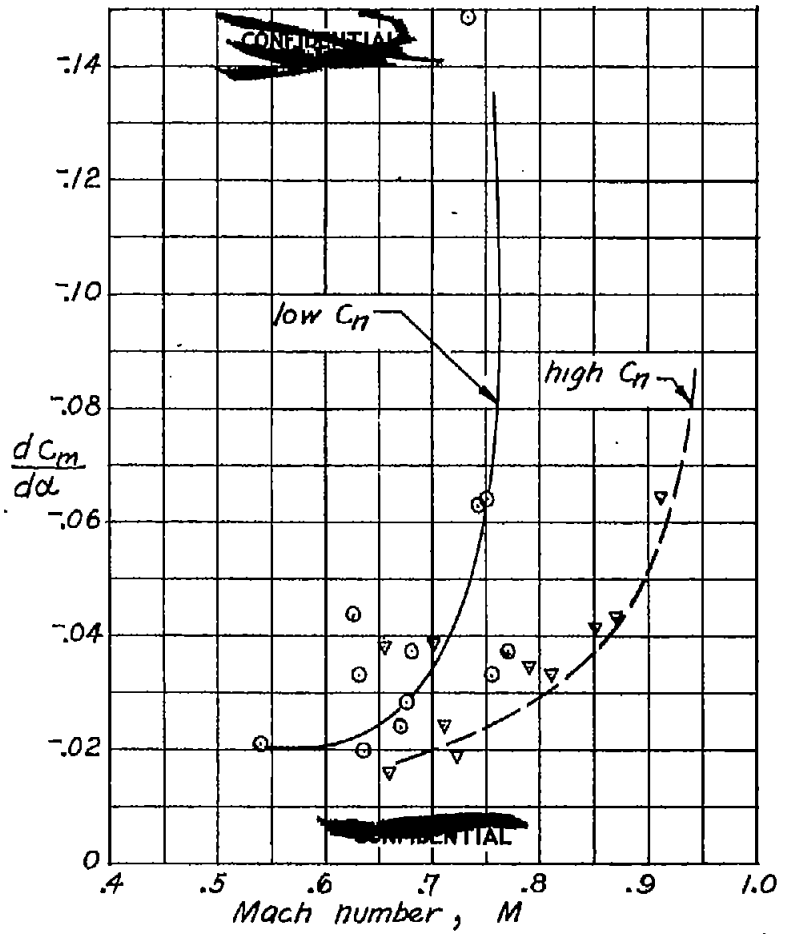

(c) Standard configuration; $\delta_f \approx 60°$

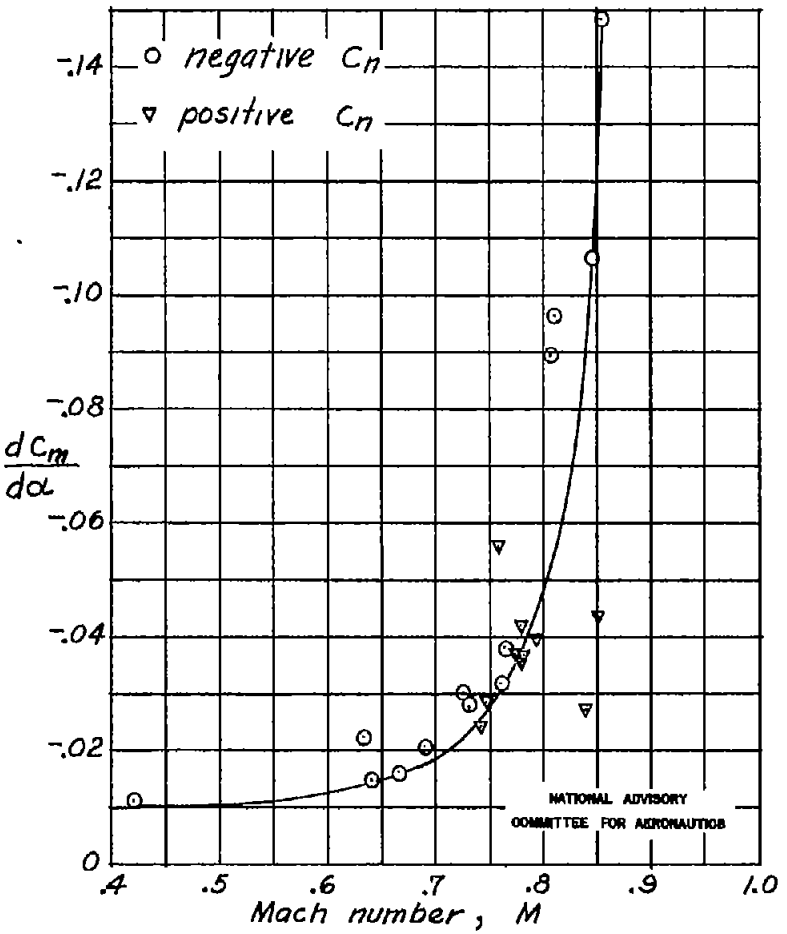

(d) Tail in line; $\delta_f = 0°$

Figure 25. - Concluded.

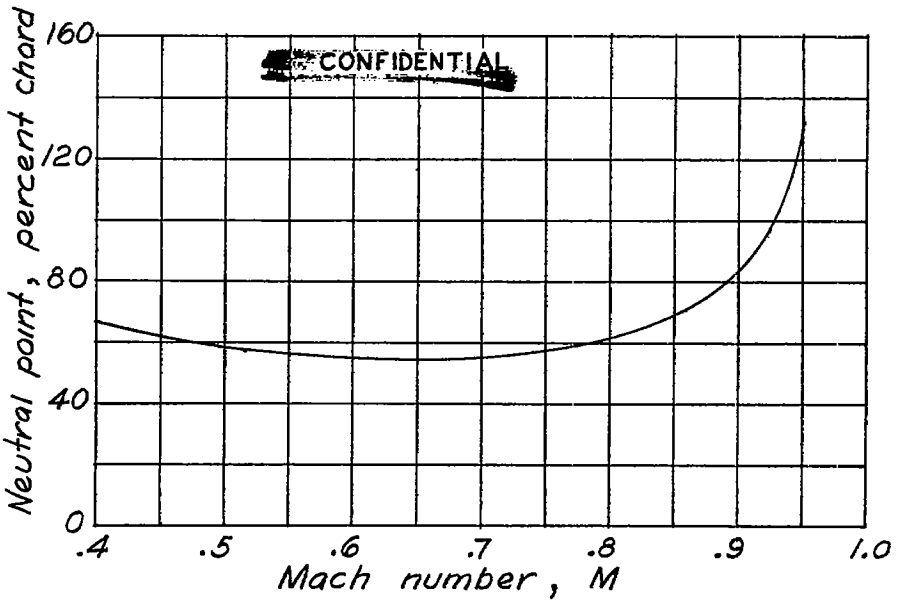

(a) Standard configuration; $\delta_f = 0°$

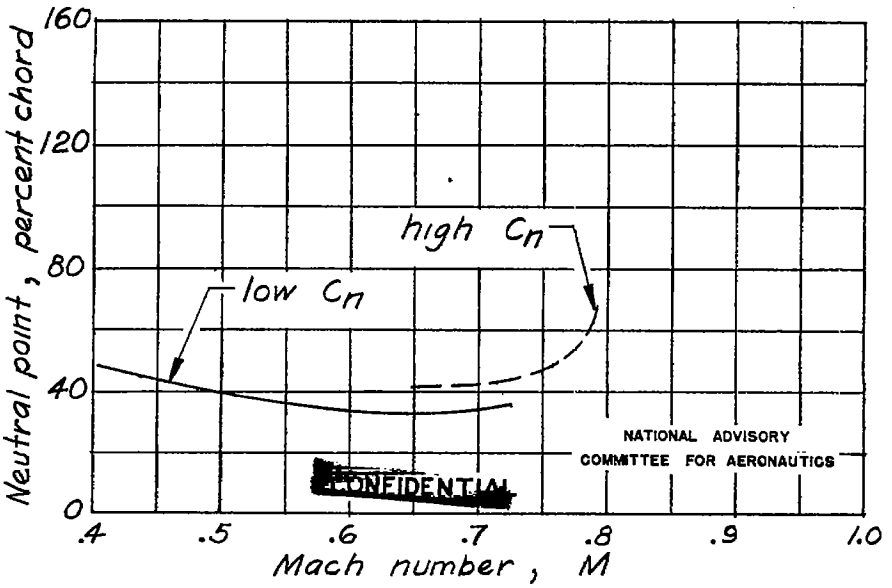

(b) Standard configuration; $\delta_f = 15°$

Figure 26. - Variation of the neutral point with Mach number.

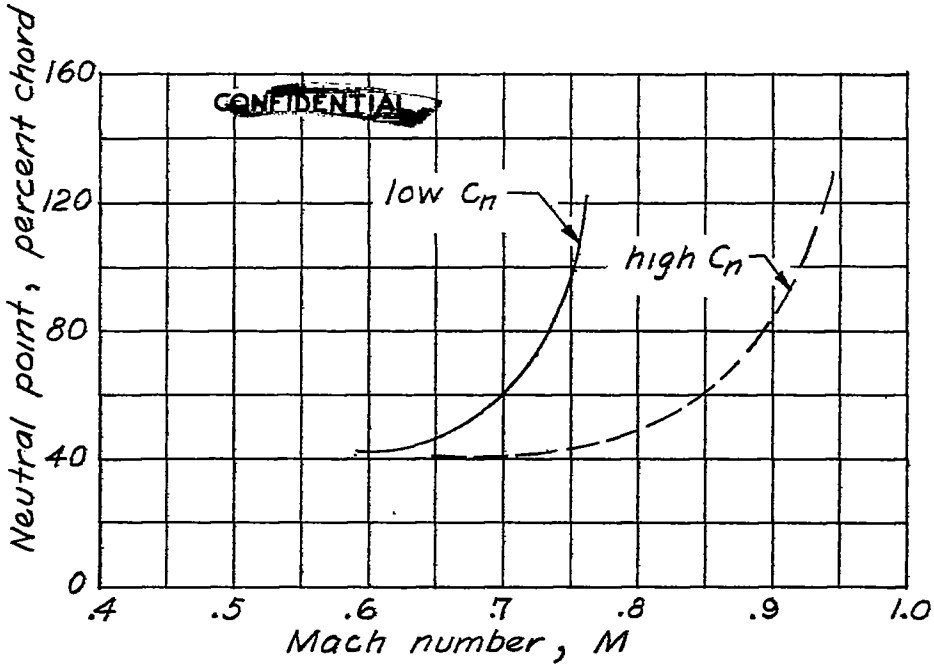

(c) Standard configuration ; $\delta_f \approx 60°$

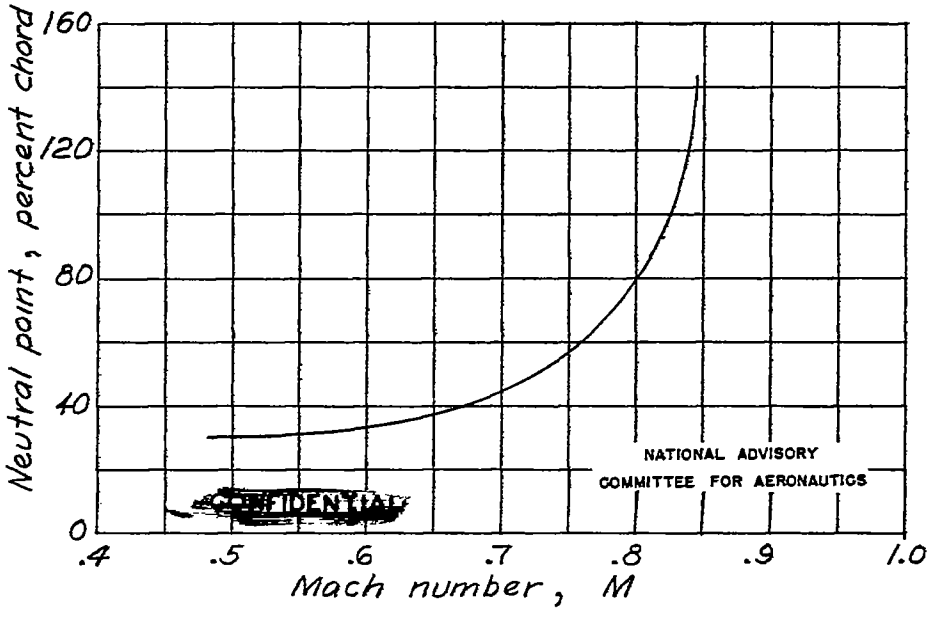

(d) Tail in line ; $\delta_f = 0°$

Figure 26. - Concluded.

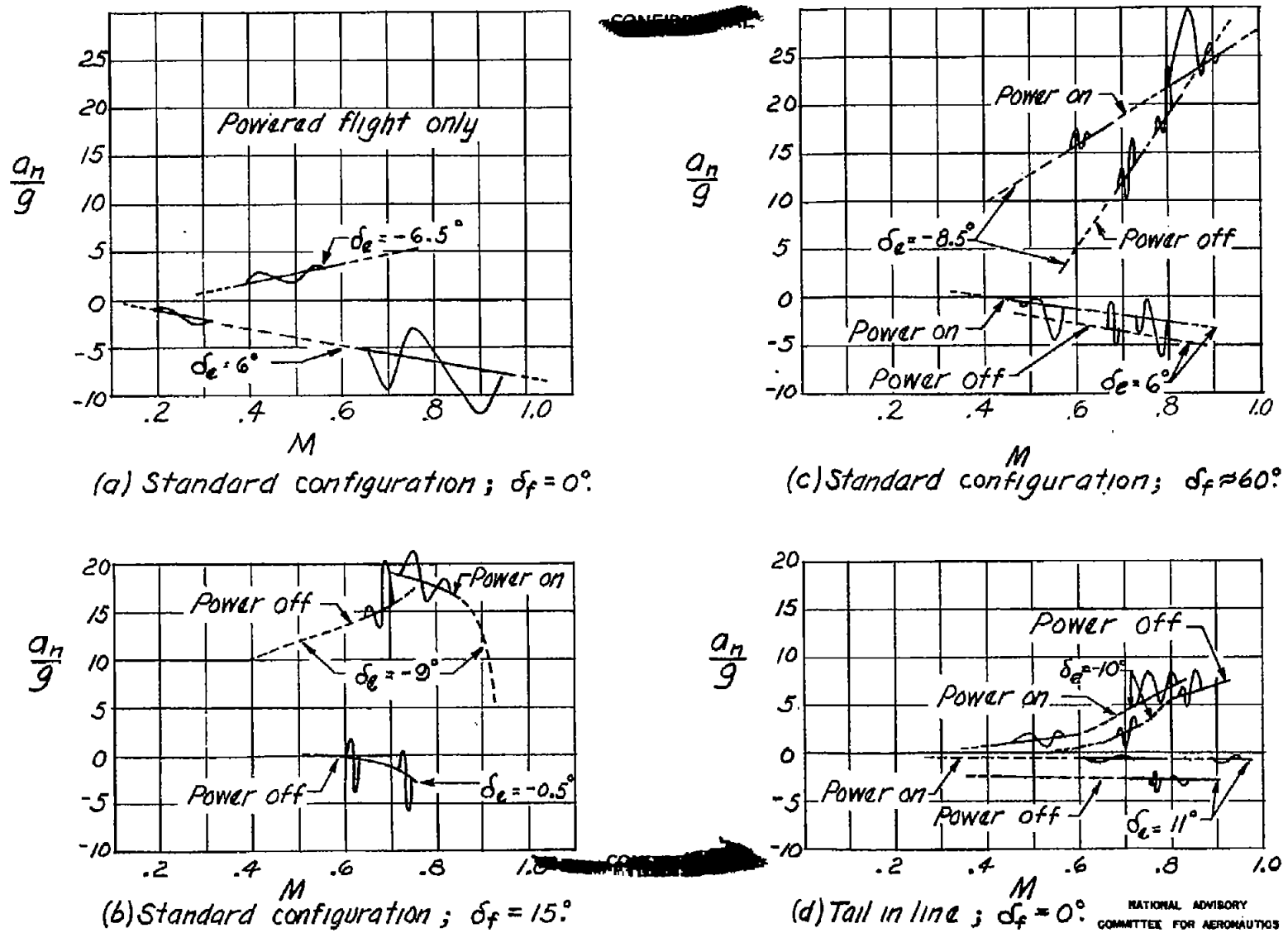

Figure 27.- Variation of normal acceleration with Mach number.

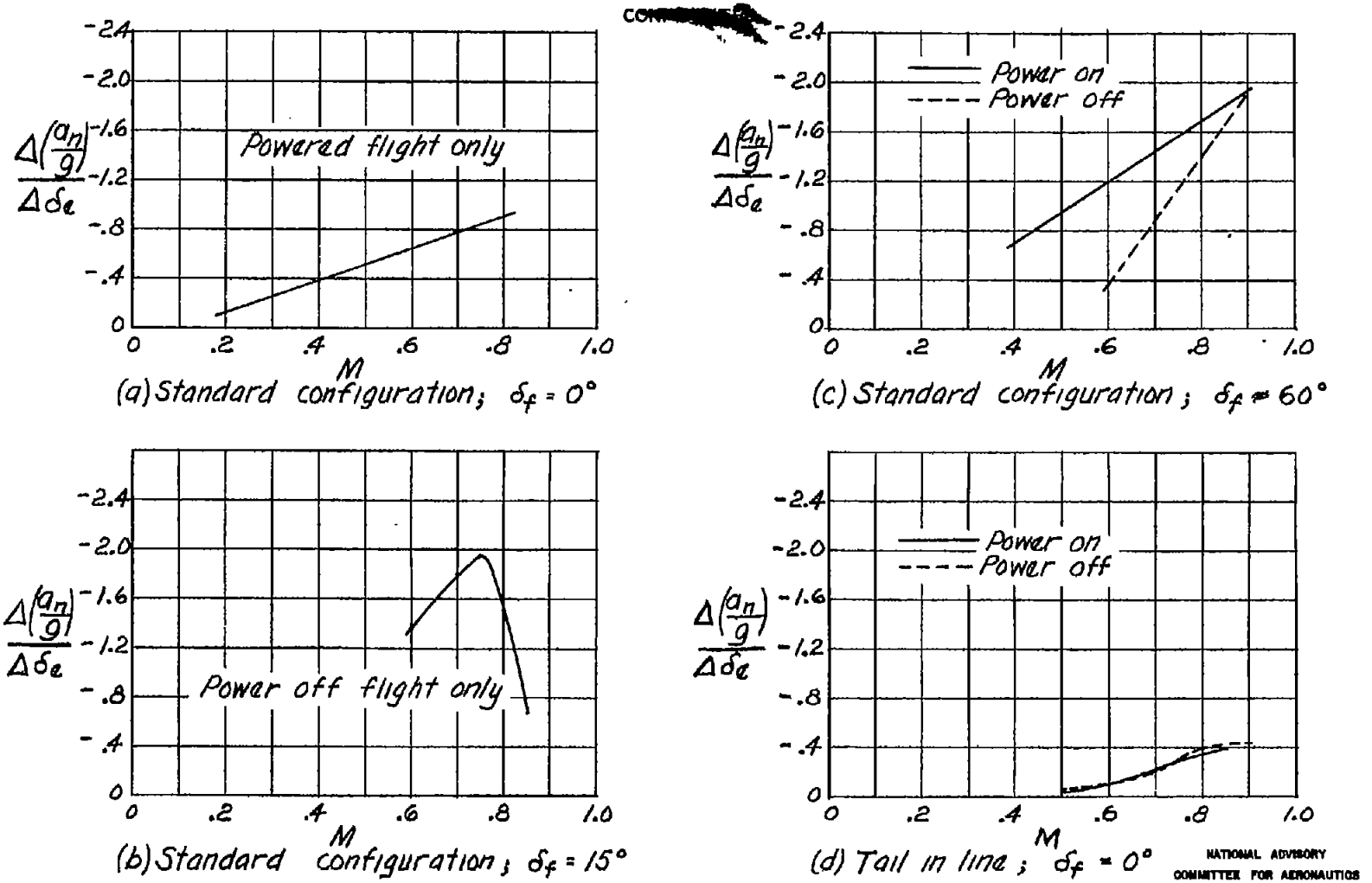

Figure 28.- Comparisons of the increment of normal acceleration produced by control deflection as a function of Mach number.

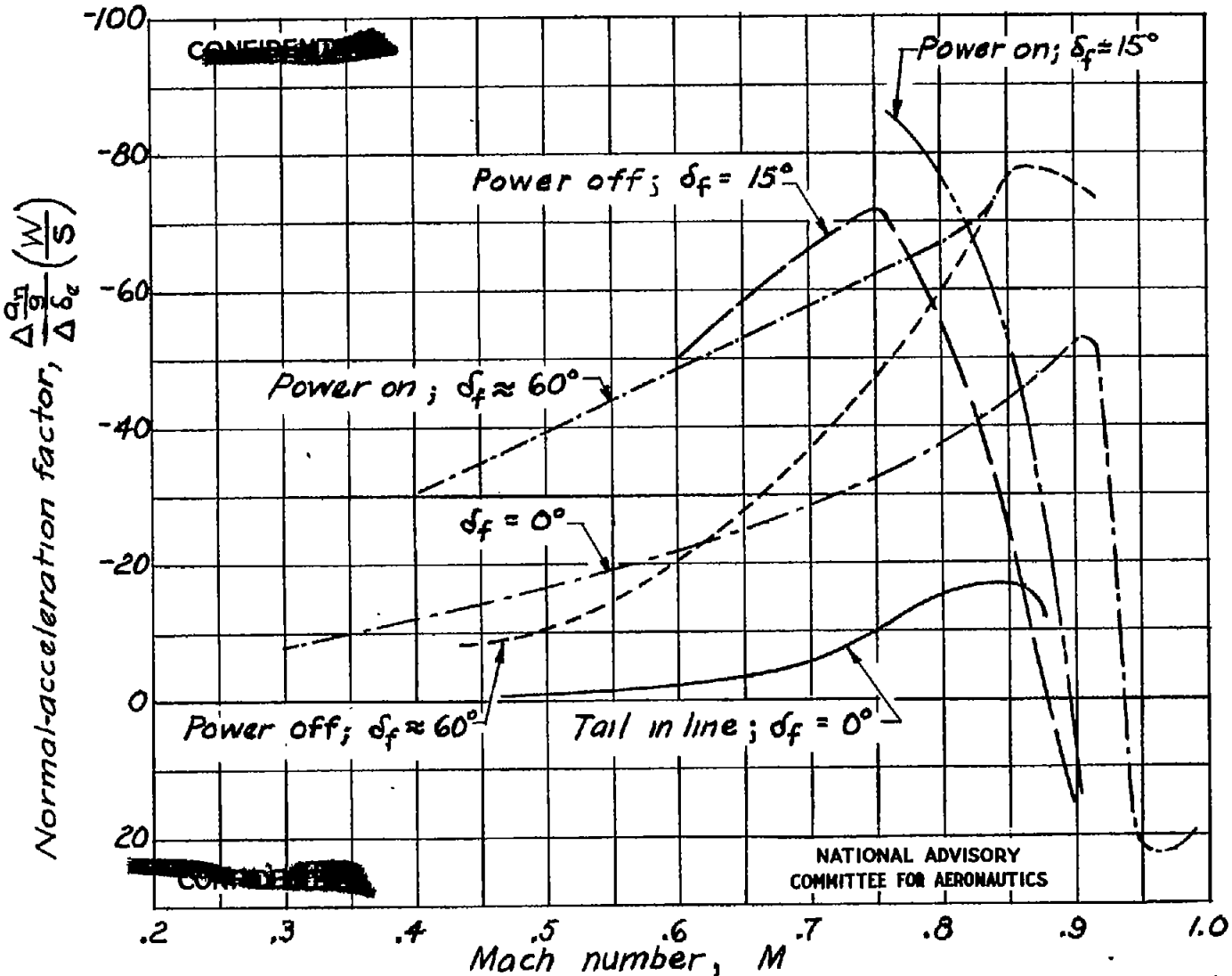

Figure 29.- Comparison of the normal acceleration producing ability of the control surfaces for all the configurations tested.